Image-based Finite Element Analysis of Head Injuries and Helmet Design

By

Zhaoyang Liang

A thesis submitted to
the Faculty of Graduate Studies of
The University of Manitoba
in partial fulfilment of the requirements for the degree of
Master of Science

Department of Mechanical and Manufacturing Engineering
Faculty of Engineering
University of Manitoba
Winnipeg, Manitoba

Dec. 2011

Abstract

Biofidelity of finite element head model (FEHM) includes geometric and material aspects. A FEHM with inhomogeneous material properties was proposed to improve material biofidelity. The proposed FEHM was validated against experimental data and good agreements were observed. The capability of the proposed model in simulating large tissue deformation was also demonstrated. Influences of inhomogeneous material properties on the mechanical responses of head were investigated by comparing with homogeneous material model. The inhomogeneous material properties induce large peak strains in head constituents, which are probably the cause of various brain injuries.

Helmets are effective in preventing head injuries. Parametric studies were conducted to investigate how changes in helmet shell stiffness, foam density and pad thickness influence the performance of a helmet in protecting the brain. Results showed that strain energy absorbed by foam component, contact stress on the interfaces and intracranial responses are significantly affected by foam density and pad thickness.

Acknowledgments

During my study in University of Manitoba, I have received guidance and support from a lot of people. Firstly, I would like to express my deepest gratitude to my advisor Dr. Yunhua Luo, who has provided me with valuable instruction in every stage of my graduate study. Without his enlightening guidance, impressive kindness and patience, I was not able to complete my graduate study. His keen and vigorous academic observations enlightened me not only in this thesis but also in my future study.

I shall extend my thanks to all my friends for their care, support and encouragement. Special thanks to Dr. Qingjin Peng, Dr. Quan Wang, Mr. Nan Wu, Mr. Dai Shi, Mr. Kevin Zhang for their valuable help in my graduate study.

My thanks also go to my beloved parents for their love and great encouragement to me through all these years. Thanks to my wife Zhenzhen Lu for her understanding and love during the past two years. Thank you very much for your deep love.

Contents

List of Tables

List of Figures

List of Abbreviations

TBI	Traumatic brain injury
FEHM	Finite element head model
FEM	Finite element method
FE	Finite element
DAI	Diffuse axonal injury
3D	Three-dimensional
CSF	Cerebrospinal fluid
SI	Structural intensity
HIC	Head injury criterion
HIP	Head Injury Power
STP	Standard temperature and pressure
HU	Hounsfield unit
mm	Millimeter
ms	Millisecond
CT	Computed Tomography
kg	Kilogram
GPa	Gigapascal

MPa	Megapascal

List of Symbols

σ	Stress
ε	Stain
t	Time
τ	Relaxation time
μ	Dashpot viscosity
E_1, E_2, E_0, E_∞	Spring constants in the standard viscoelastic model
G, G_∞, G_i, G_0	Shear modulus
G, K_∞, K_i, K_0	Bulk modulus
υ	Possion's ratio
$E, E_{11}, E_{22}, E_{33}$	Young's modulus
ρ_{brain}	Brain mass density
$\rho_{cortical}$	Cortical bone mass density
$\rho_{cancellous}$	Cancellous bone mass density
$E_{cortical}$	Young's modulus of cortical bone

$E_{cancellous}$	Young's modulus of cancellous bone
E_{brain}	Young's modulus of brain tissue
υ_{bone}	Bone Possion's ratio
υ_{brain}	Brain tissue Possion's ratio

List of Copyright Materials

Fig. 1 on page 4 was revised from website ‘http://www.fmrib.ox.ac.uk/education/fmri/images/sagittal_scan.jpg/view’. Copyright was obtained on Oct. 2011.

Fig. 2 on page 6 was cited from ‘Kleiven, S., Finite element modeling of the human head. Ph. D, Department of Aeronautics, Royal Institute of Technology, Stockholm, 2002’. Copyright was obtained on Nov. 2011.

Table 5 on page 54 was cited from ‘Kostopoulos, V., Markopoulos, Y. P., Giannopoulos, G., and Vlachos, D. E., Finite element analysis of impact damage response of composite motorcycle safty helmets. *Composites: Part B*, vol. 33, pp. 99-107, 2002’. Copyright was obtained on Feb. 2012.

Fig. 5 on page 23 was reproduced from ‘Davis, G., Kohandel, M., Sivaloganathan, S., and Tenti, G., The constitutive properties of the brain paraenchyma Part 2. Fractional derivative approach. *Medical Engineering & Physics*, vol. 28, pp. 455-459, 2006’. Copyright was obtained on Feb. 2012.

Fig. 29 on page 55 was cited from ‘Viot, P., Hydrostatic compression on polypropylene foam. International Journal of Impact Engineering, vol. 36, pp. 975-989, 2009’. Copyright was obtained on Dec. 2011.

Fig. 30 on page 55 was cited from ‘viot, P., Maheo, L., and Mercier, A., Behaviour of polymeric multiscale foam under dynamic loading-study of the influence of the density and the walls of beads. International Journal of Research and Reviews in Applied Sciences, vol. vol. 7(1), pp. 1-19, 2011’. Copyright was obtained on Jan. 2012.

Chapter 1

Introduction

1.1 Background

Traumatic Brain Injuries (TBI) are one of the main causes of death or permanent disability in daily life. The brain is the center of the human body's nervous system and consists of billions of nerve cells connected to other parts of the body. Any damage to the brain will affect the functionalities of all other parts of the body. Although protected by the skull, the brain is very vulnerable to impacts. The increased use of mobile vehicles in daily life is the main cause of brain injuries [1]. A survey conducted in 1998 shows that traffic accidents were the leading cause of death for individuals aged from 1 to 34 years in the United States [2]. In the European Union countries, there were about 45000 reported fatalities and 1.5 million casualties in 1995 [3]. Despite the use of protection equipment such as belts, air bags and helmets, and stricter governmental regulations, traffic accidents were still responsible for about 40% of all TBI cases in the United Kingdom in 1997 [4]. TBI not only causes serious disabilities to individuals, such as long-term headache, vision or hearing problems, sleep disorders and mood changes, but also causes an

enormous burden to society, especially the medical system. Direct medical costs and indirect costs were estimated $60 billion in the United States in 2000 [5]. Since TBI is now a serious public health problem, the mechanism of how an impact to the head causes brain injuries has to be understood. Because of the limitation and ethnic problem involved in experiment studies, the finite element method (FEM) is widely utilized to study the biomechanics of TBI.

Helmets have been proven effective in reducing the incidence and severity of head injuries in accidents. For instance, motorcycle related deaths were reduced by 29% during 1972-1987, while during 1993-2000 the reduction was further increased to 37% due to the improvement in helmet design and advances in materials [6]. The typical structure of a helmet includes two layers: the stiff outside layer, and a relatively soft inner layer. Changes in the mechanical properties of the two layers will affect helmet performance. Improving the design of helmet to reduce brain injuries is an important research topic in Biomechanical Engineering.

1.2 Objectives of the Reported Research

The objective of this thesis is to develop a three dimensional (3D) finite element head model (FEHM) with improved material biofidelity to study the mechanical mechanisms of brain injuries. The ability of the developed model in predicting brain injuries and the influences of inhomogeneous material properties on the model will be investigated. After the validation of the 3D FEHM, the head model is used in parameter studies of helmet

design. The influences of shell stiffness, foam density and foam thickness are studied to improve helmet design.

1.3 Basic Anatomy Structure of Human Head

To understand the mechanical mechanisms involved in brain injuries, the basic anatomical components of a human head are introduced in this section. Generally speaking, the human head can be simplified as a four layers structure separated by the skin, skull, brain, and meninges [7]. The stiff skull bone provides a major protection to the brain from foreign object penetration. It can be viewed as a three-layered sandwich structure. The inner and outer tables are stiff compact bone, and the middle layer is the relative soft diploe. Between the brain and skull are three other protective coverings, they are membranes named dura mater, arachnoid, and pia mater. They enclose the brain, spinal cord, and the central nerves system. These meninges consist primarily of connective tissues, and they form part of the walls of blood vessels and sheaths of nerves. Between the arachnoid and the brain is cerebrospinal fluid (CSF) bathing and circulating around the brain. It cushions the brain and spinal cord during impact. However, it cannot constrain the brain from motion relative to the skull [8]. As an additional protection, there are fibrous filaments known as arachnoid trabeculations, which extend from the arachnoid to the pia and bridge the brain to prevent it from excessive movement in cases of sudden acceleration or deceleration [1].

The brain consists of the cerebrum, cerebellum and brain stem. The brain is partly separated into the left and right hemispheres by the falx cerebri. The tentorium separates the

cerebrum from the cerebellum and brain stem and connects to the dural membrane (Fig. 1). The cerebrum is the largest part of the brain. Each hemisphere is divided into four lobes: the frontal lobe, the temporal lobe, the parietal lobe and the occipital lobe. The outer layer of the cerebrum consists of gray matter and white matter. An important part of the white matter is the corpus callosum which connects the two hemispheres of the cerebrum. The brain stem connects the brain with the spinal cord and it goes through the foramen magnum.

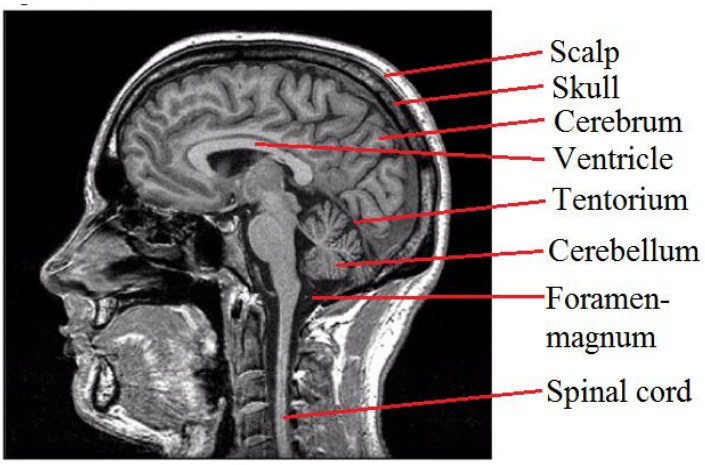

Fig. 1 Para-sagittal section view of human head (modified from [9])

1.4 Brain Injury Mechanisms

Based on clinical observations, brain injuries can be classified into two categories: focal injuries and diffuse injuries. Focal injuries refer to local damages to the brain usually accompanied by bleeding, while diffuse brain injuries involve the rupture of brain tissues, which are usually invisible [10]. Epidural hematomas, subdural hematomas, and contu-

sions (coup and contrecoup) are the general forms of focal injuries, while diffuse injuries comprise of brain swelling, concussion, and diffuse axonal injury (DAI) [11] .

1.4.1 Focal injuries

Focal injuries are characterized by bleeding within the skull. They more commonly appear when the head strikes, or is struck by an object. Focal injury may or may not be accompanied by skull fractures. Epidural, subdural, and subarachnoid bleedings are usually signs of focal injuries in the spaces between the meninges. Blood clot that develops outside the dura, between the skull and dura, is known as epidural hematoma. When it develops between the brain and the dura, is called subdural hematoma. Blood leaking into CSF is known as a sub-arachnoid hematoma. Among all these focal injuries, the most common one is contusion (coup-contrecoup) brain injury. The CSF acts as a cushion to provide protection to the brain. Nevertheless, due to its fluid-like property, it cannot sustain the shear stress/strains. During an impact, the translational cranial motion causes relative brain movements with the skull; as a result, the brain parenchyma is displaced away from the site of the skull impact (coup) and toward the opposite (contrecoup) site resulting in the more severe brain contusion (Fig. 2). Coup contusion is induced by a slapping effect of the skull hitting the brain; while the bouncing of the brain against the inner posterior surface of the skull and the possible development of cavitation bubbles within the brain due to high negative pressures would cause the contrecoup lesions [12-14]. The growth and collapse of these bubbles are very harmful to brain vessels and are one of the possible reasons for the local tissue damages. This phenomenon is also known as contre cavitation or negative pressure theory.

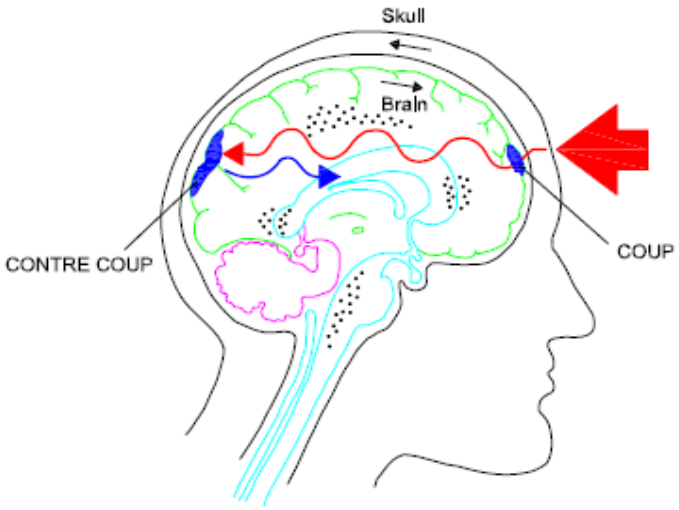

Fig. 2 Dynamics of coup-contrecoup injury [8]

Another theory advocated by several authors to explain this coup-contrecoup phenomenon is the shear strain theory [13, 15]. Because of high water content (about 80%) in the brain, it is considered as nearly incompressible. The dynamic bulk modulus of brain tissue is about 2.1 GPa which is approximately 10^5 times larger than the shear modulus [8]. Thus, damage of brain tissue is determined mainly by shear strength of brain tissues. Shear strains/stresses induced during the impact process are the major cause for the rupture of bridging blood vessels.

However, these theories are still controversial, and some of them don't conform to the clinical observations [16]. For example, in substantial autopsy studies, for all the cases that have receieved a blow to the head, only one presents a contre-coup lesion [17]. During the contre-coup lesion, desipte the negative pressures are observed at the contre-coup site, they often may not be high enough to cause damage to the brain [18, 19].

1.4.2 Diffuse injuries

Unlike focal injuries which can be observed by naked eyes or visualized by the CT scans, diffuse damages are on the cellular level. Diffuse injuries have the common forms as edema, DAI and concussion. Edema is resulted swelling of the brain; it becomes dangerous when the swelling causes a considerable increase in the intracranial pressure which can prevent blood from entering the skull to deliver glucose and oxygen to the brain. Concussion, which is the most common head injury diagnosed, involves immediate loss of consciousness. DAI is accompanied by ruptures of long nerve fibres called axons in the cerebral hemispheres and white matter. Billions of nerve cells which are connected with distant nerve cells through axons located in the gray matter. Severe sudden twisting or torqueing of the brain, as occurred in a sudden acceleration/deceleration-whiplash-accident, can stretch, twist, and damage these axonal fibres. Depending on the locations of damages, DAI has three stages of lesions [20]. Stage 1 lesions usually locate at the gray-white matter junction. Stage 2 lesions involve the corpus callosum. Stage 3 lesions are the most severe and involve the brainstem.

Mechanical mechanisms of diffuse injuries are still not fully understood by researchers. A rotational acceleration which results in the shear stress/strain contributes to both focal and diffuse brain injuries, while linear acceleration is considered as the cause of focal brain injuries. However, King et al. [21] proposed that the large strain rate was a better indicator of the brain injuries than the stress/strain or pressure gradient theory. Understanding of the brain injury mechanisms needs both improvement at the experimental techniques and clinical observation technologies.

Chapter 2

Three-Dimensional Finite Element Head Model with Improved Material Biofidelity

2.1 Introduction

Biomechanics of brain injuries caused by impact is a 3D dynamic problem. The internal biomechanical responses of the brain, i.e. the transient stress distributions induced by the dynamic loading, cannot be completely measured by experimental techniques. Sensors for measuring stresses and strains cannot be installed in the brain. Hence, other methods are developed, for example, analytical modeling and numerical simulation.

Analytical models are based on the principle of mechanics and produce solutions to head impact problems by solving a set of mathematical governing equations [22-24]. However, this approach is limited to relatively regular geometry, simple boundary conditions and homogeneous material properties, due to mathematical difficulties in formulation and solution of the governing equations.

The FEM implemented in computer codes is an efficient numerical procedure for producing approximate solutions to complex problems such as head injury analysis. In principle, the FEM uses piece-wise polynomials to approximate the original continuous unknown field functions. The geometrically complex problem domain is represented by finite elements. The domain occupied by the head model geometry is discretized into a finite number of elements. The advantage of FEM over the other methods is that it can include irregular geometry, inhomogeneous and nonlinear material properties and complex boundary and loading conditions. For a given mechanical impact, the finite element (FE) analysis can predict stress/strain distributions in the brain.

Head injuries are caused by excessive stresses or strains induced by impact. Identifying the correlation between mechanical responses of brain tissue induced by impact and the neurological and pathological symptoms is the ultimate objective for biomechanical studies of brain injuries. For example, phenomena such as contre-coup lesion and DAI are accompanied by the large pressure and stress/strain distributions. The large relative motion between the brain and the skull may cause subarachnoid haemorrhage when the head acceleration reaches a certain magnitude [25].

2.2 Existing Finite Element Models for Studying Brain Injuries

During the last few decades, different FE models of the head have been developed to obtain a better understanding of the mechanical responses of human head under different dynamic loadings. The developed FE models have shown a great improvement handling in geometric complexity with advances in computer technology. In the following sections, a brief review is conducted on the recently developed 3D FEHM used for brain injury analysis.

2.2.1 Finite Element Models Including Different Anatomical Parts of the Head

Ward and Thompson [26] in 1975 developed one of the first 3D FEHM to replicate the experiment results from cadaver tests. The major components of a head were included in their model. The brain tissue was represented by 189 eight-node brick elements. The dura mater, falx and tentorium membranes were modeled by 80 four-node shell elements. The skull was modeled as a rigid body, while the CSF and brain were modeled as a linear elastic material. In 1982, a brain FE model was developed by Ward [27]. The membranes and fluid were included, while the skull was not. He found that the internal folds of dura, falx influenced the mechanical responses of brain, the high normal stresses caused serious brain injury, and the combined tension and shear stresses produced subarachnoid haemorrhage.

In 1993, Ruan et al. [28] developed a FEHM which was the first version of the Wayne State University brain injury model. It included the scalp, skull, brain, dura mater and

falx cerebri. In his model, the brain was modeled as a visco-elastic material. In 1995, Zhou et al. [29] presented a detailed FEHM based on Ruan's work. The grey and white matter, ventricles inside the brain and the bridging veins were introduced in this model. The FE mesh was also considerably refined. The numerical model was validated by comparison with the intracranial pressure data from Nahum et al. [30]. The shear stress distributions in brain were found to be affected by this inhomogeneous brain (grey and white matter) and the inclusion of ventricles. They believed that shear strain levels in the corpus callosum is a predictor of DAI and the occurrence of subdural hematoma was closely related to the impact direction. Zhang et al. [31] later improved the Wayne State University brain injury model, by introducing the sliding interface between the skull and the brain and refining the model with much finer meshes. The new version of the Wayne State University brain injury model consisted of all essential anatomical features of a 50^{th} percentile male head, including the scalp, skull with an outer table, diploe, inner table, dura, falx cerebri, tentorium, pia, sagittal sinus, transverse sinus, CSF, white and grey matter, cerebellum, brainstem, lateral ventricles, third ventricles and bridging veins. A facial model composed of 14 facial bones was also included to simulate features of the human face. The brain was characterised as viscoelastic, and elastic-plastic material model was used for cortical and cancellous bones of the head. This FEHM was used to study the minor traumatic brain injury sustained by American football players.

Kang et al. developed the University Louis Pasteur FEHM in 1997 [32]. The geometry of the skull was constructed by digitising a human adult male skull. The main anatomical features were modelled, i. e., the skull, falx, tentorium, subarachnoid space, scalp, cere-

brum, cerebrum, cerebellum and brain stem. An elastic material model was used for the brain-skull interface. Material properties of the CSF, scalp, facial bones, tentorium and falx were all isotropic and homogeneous, while the brain was assigned with viscoelastic properties. The University Louis Pasteur head model was evaluated by simulating Nahum's cadaver head impact test. In 2004, Deck et al. improved this FEHM by composing a detailed complex geometry of a skull, including the evolution of the skull thickness throughout the skull and, for the first time, the reinforced beams which play an important role in its dynamic response to impact [33].

In 2002, Kleiven and Hardy [34] proposed a detailed and parameterised FE model of the adult human head, namely the Kungliga Tekniska Hosgskolan FEHM. A simplified neck, including the extension of the brain stem to the spinal cord, the dura mater, spine, muscle and skin, were modelled. Geometries of these tissues were extracted based on the contours of the color photos from the Visible Human Database. The number of elements and mesh density can be changed as desired; this feature makes this FE model parameterised.

Takhounts and Eppinger in 2003 proposed the simulated injury monitor FE model [35]. It consisted of the rigid skull, the dura-CSF layer, the brain, the falx cerebri and the bridging veins. The brain was simplified in order to save the run-time. The region under the brain and the tentorium was modelled as a continuation of the dura-CSF layer and did not represent either the cerebellum or the midbrain. The skull was assumed to be rigid, whereas the rest of the head was considered as deformable, linear viscoelastic, isotropic, and homogeneous. This model was used to replicate 24 cases of 1712 impacts in college football to investigate the potential TBI. The injury metrics such as cumulative strain

damage measure, relative motion damage measure, and dilatational damage measure were established based on these measured data.

Zong et al. develop a 3D FEHM in 2006 [36]. In his model, the brain was modeled as a homogeneous material. The CSF was modeled by a material whose Poisson's ratio was near 0.5 and behaved like an incompressible fluid. The neck was modeled as three parts, spinal cord, cervical bone and disc. The Structural intensity (SI) methodology was introduced to assess the injury likelihood of the head subjected to impact loading. SI was a vector quantity indicating the direction and magnitude of energy flow inside the head. Three cases, namely frontal, rear and side impacts were studied to compute the SI distribution in the head. He found that the spinal cord suffered from strong wave motion and had high SI distribution during the impact. Thus, the high possibility of spinal cord injury was more related to wave motion inside the head. He suggested that the protective equipment was effective when the impact force was reduced to such an extent that no severe strong wave motion was built inside the head.

Based on recent advances in medical imaging techniques and in computational methods, voxel-based finite element head model was developed to investigate mechanisms of head injuries. In 2008, Watanabe et al. developed a voxel-based FEHM [37]. This model was established by converting the voxel in CT images to FE meshes, and it consisted of 1.22 million hexahedron elements and 10 tissues. The simulation of the head subjected to a lateral rotational impact was conducted to understand the mechanism of DAI. The obtained results showed that larger stresses occurred in the brain stem and cerebral limbic system accounted for the DAI.

Y. Chen and M. O. Starzewski developed a FEHM through an efficient magnetic resonance imaging (MRI) voxel-based mesh generation method [38]. This 3D FE model of the human head was able to capture the important geometric characteristics of the various components within the human head. The thin CSF layer was modeled by a homogenized solid material with bulk modulus of 21.9 MPa and shear modulus of 50 KPa. These values of moduli indicated the CSF layer was much more sensitive to the shear strain/stress. The brain tissues were modeled as viscoelastic materials with strong strain rate dependence.

2.2.2 Finite Element Models Considering Interfaces between Head Tissues

Of all the interfaces among head tissues, the skull-brain interface is the most important one. There are many blood vessels in the space between the skull and the brain. Excessive relative motion between the brain and the skull may result in rupture of vessels. Several methods for modeling the skull-brain interfaces are proposed in the literature. The simplest one is to connect the skull and the brain using a set of nodes connected to the two tissues [38-40]. This method is easy to be implemented, but it does not allow relative motion between the brain and the skull. In order to simulate the relative motion, solid elements with low shear modulus were used to represent the space filled by CSF [29, 32, 41].

Contact models were also utilized to simulate the kinematic and kinetic behaviour between surfaces of the skull and the brain. The mechanical behaviour of interface was

modelled by a number of degrees of freedom in the relative tangential and normal direction of the skull and the brain. In some models only tangential motion between the brain and the skull is allowed [42]. Both of the tangential and the normal separation motions were simulated by Kuijpers et al. [43] and Ueno et al. [44]. Tangential interaction between the skull and the brain is modeled as slip with different friction coefficients or as frictionless motion in different models [45]. A failure criterion is employed to specify to what extent the skull and the brain can be separated [46].

2.2.3 Validation of FEHMs

After the establishment of FEHM, the next critical step is the validation of the head model. Only when the FEHM is validated against experiment results, the results produced by FEHM can be considered as reliable.

One way of validation is based on modal analysis [45, 47, 48]. Modal analysis provides dynamic characteristics of the system under consideration. Nature frequencies and corresponding vibration modes of the whole head system can be determined by experiments. If the calculated eigen-frequencies are equal or close to the measured data, the FEHM is reliable.

The second way for validating FEHM, which is the most popular one in the literature, is based on comparison of intracranial pressure. Two cadaveric experiments were conducted by Nahum et al. [30] and Trosseille et al. [49] respectively. In Nahum's experiment, a seated human cadaver was impacted by a 5.6 kg impactor at a velocity of 9.94 m/s. Intracranial pressure data at five locations, i.e., coup (impact site), contrecoup (opposite impact site), parietal and two occipital sites, were recorded. This head impact test measured

the transient information of the head in terms of local pressures. Because of the short duration of the impact (approximately 6 ms), the support from the neck was considered having trivial effect on kinematic responses of the head [38, 50]. A free-boundary condition, meaning there is no constraint at the head-neck joint, is usually employed. In Trosseille's experiment, the general preparation of the cadavers was similar to those in Nahum's experiment. Six tests involving three cadavers were conducted. The cadavers were impacted by a 23.4 kg impactor at a speed of 7 m/s. The 3D head kinematics was measured by accelerometers installed onto the skull. The pulse duration in his experiment was about 15 ms, therefore, neck support would have effect on the kinematic responses of the head.

Unlike in the previous experiments, Hardy et al. [51] measured the relative brain motion with respect to the skull using a high-speed, bi-planar x-ray system and neutral density targets. In his experiment, each cadaver was subjected to multiple tests, either struck at rest using a 152 mm diameter padded impactor, or stopped by an angled surface from a steady-state motion. An array of multiple neutral density targets were implanted in two columns, each had 5 or 6 targets, with a distance of 10 mm between targets in a column and 80 mm between columns. These targets were implanted in the temporoparietal and occipitoparietal region. The subsequent relative displacement of each neutral density target was used in FEHM validation.

Due to the difficulties involved in tracking the various localized dynamic behaviour of the head, available experimental data are also very limited. It is obvious that tissue conditions in a cadaver are different from those in vivo. Therefore, experimental data obtained by cadaveric experiments can only provide a qualitative validation for FEHM.

2.2.4 Injury Criteria

Based on FE solutions, injury criteria are developed for predicting head injuries. Head injury criterion (HIC) developed by Versace et al. [52] uses head translational accelerations to predict head injury. The criterion is expressed as

$$HIC = [\{\frac{1}{(t_2 - t_1)}\int_{t_1}^{t_2} a(t)dt\}^{2.5}(t_2 - t_1)]_{\max} \quad (1)$$

Where $a(t)$ is the resultant linear acceleration, t_1 and t_2 are the starting and ending instants of the interval (in seconds) during which the head sustains the acceleration. HIC is a good indicator for brain injuries in some cases [53]. However, poor correlation between HIC and injury severity has been found in various directional impacts [54]. The main drawback of HIC is that the rotation accelerations of the head are not considered. Due to the convenience of measuring head accelerations than measuring intracranial response, HIC has been adopted in safety standards of head protection devices.

Newman et al. [55] proposed another head injury criterion called Head Injury Power (HIP). The HIP criterion given in Eq. (2) is based on the change rate of translational and rotational kinetic energy. It includes all the six degrees of freedom of motions. The maximum value of the function during the impact represents the maximum power input to the head and serves as a standard by which the probability of head injury can be assessed.

$$HIP = \sum m \cdot a_i \cdot \int a_i dt + \sum I_{ii} \cdot \alpha_i \cdot \int \alpha_i dt \quad (2)$$

Where m is the mass of the head (kg), a_i is the linear acceleration (m/s^2), I_{ii} is the moment of inertia ($kg \cdot m^2$), and α_i is the angular acceleration (rad/s^2).

HIC and HIP provide an estimation of the injury risk of external mechanical loadings based on the acceleration data, but they do not take into account the internal mechanical response of the head. More accurate prediction of brain injuries can be done by using intracranial mechanical responses obtained from finite element simulations. One example is provided by Takhounts et al. [35]. The developed injury predictive criteria such as cumulative strain damage measure, relative motion damage measure, and dilatational damage measure are used for evaluating DAI, acute subdural hematoma, and contusions [35].

2.3 Construction of Geometric Model of the Head

With the aid of medical images, the geometric biofidelity of head model has been greatly improved by including as many head components as possible. Basically, there are two methods to construct the geometric model of the head, surface-based method [35, 36, 50] and voxel-based method [37, 38]. The general procedure of the surface-based method is briefly described here. First, a set of thresholds is defined to distinguish tissue components from medical images; secondly, the boundary surfaces are extracted to form the geometry of each component; and then the head components are assembled to form the whole head model. This method has many drawbacks. The main one is that it will lead to very poor mesh quality. Boundary surfaces are key components for constructing the geometric model. However, the geometry of surfaces of head tissues is very complex due to the complicated anatomic structure of the head. The complex geometric model brings challenges to generating high quality meshes, and thus affects the accuracy of FE solutions. In order to improve mesh quality, some small geometric characteristics have to be

ignored. For instance, the folding surface of the cerebral cortex, and the non-uniform distribution of CSF layer are modelled as uniform surfaces. However, the irregular surfaces of these head tissues influence the distribution and the magnitude of maximum stress and strain in the brain when subjected to impact [33, 56]. Besides, construction of a geometric model to include all head tissues is very time-consuming.

In the voxel-based method, image pixels are directly converted into finite elements. In this method, head tissues still need to be segmented. The pixels located within the corresponding component are converted into finite elements. The huge number of elements is the main problem of this method. About 1.22 million hexahedron elements are required to represent the head [37]; even only the skull and the brain are considered, more than one million of finite elements are needed [38]. The large number of elements will greatly decrease the computational efficiency.

2.4 Material Properties of Head Tissues

To avoid these drawbacks, a non-segmentation method is introduced here to set up the head model. The outmost surface of the head is extracted from medical images, and the solid geometric model is established based on this surface model. Finite elements are generated in ANSYS from the geometric model. In the non-segmentation model, interior details of head tissues are not included. Different head tissues will be represented by assigning different material properties. In the following section, the procedure for mapping material properties from medical images to FEHM will be introduced.

2.4.1 Segmentation of head components

Once the FE mesh is generated, the FE model requires assignment of material properties. Different mass densities expressed as HU values in medical images represent different head tissues. Distilled water has zero HU at standard temperature and pressure (STP); the air has HU of -1000 at STP. HU distribution across one slice of CT image of the head is plotted in Fig. 3.

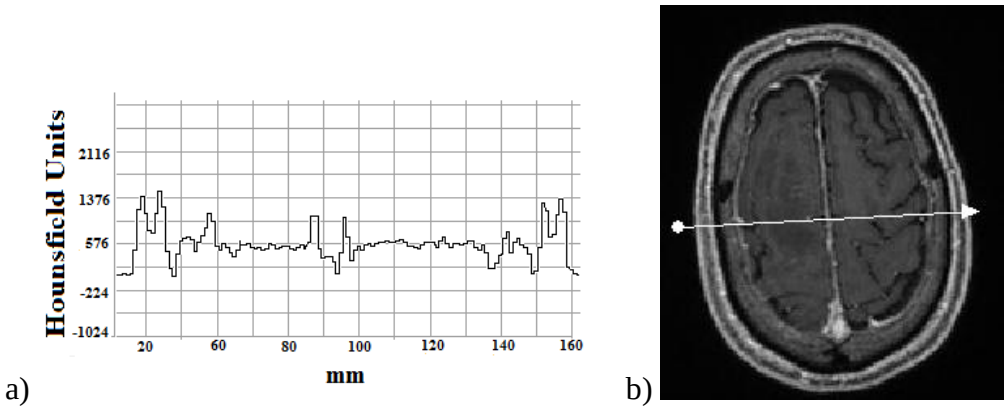

Fig. 3 a) HU distribution along one CT section b) the corresponding CT image

The head model is approximately divided into four main components according to the HU distribution, i.e., the skull, the brain tissue, the CSF and the others. The HU value of the skull cortical bone is in the range of [1255, 1955], while the HU range of the skull cancellous bone is in [755, 1255]. The HU ranges of the rest components are listed in Table 2. After the segmentation of different components, the next step is to relate these HU values to the mechanical properties.

2.4.2 Viscoelastic Material Model for Head Tissues

From the point view of engineering materials, the soft brain tissues behave like a soft gel. The mechanical behaviour of the gel-like brain can be described by the viscoelastic material model. Viscoelastic materials exhibit both viscous and elastic behaviour when they are subject to loading and undergo deformation. The viscous behaviour is like the gradual deformation of grease, and the elasticity is like a rubber band that stretches instantaneously and quickly returns to its original state once the load is removed [57]. This mixed behaviour of elastic and viscous components can be represented by a spring and a dashpot working in series or in parallel. One distinct characteristic of a viscoelastic material is the time dependence of their mechanical behaviour. The time-dependence behaviour of viscoelastic materials can be studied by means of two types of experiments: creep and stress relaxation [58].

Creep is a slow continuous deformation of a material under constant stress. Relaxation is the behaviour that when a viscoelastic material is subjected to a constant strain, the stresses in the material gradually decrease. The stresses/strains in a viscoelastic material may vary significantly with time even though the applied loads and boundary conditions are kept unchanged. To describe the viscoelastic behavior of materials, there are three basic mathematical models, the Maxwell model, the Kelvin model and and standard linear solid model [59]. To more accurately describe the behaviour of a specific viscoelastic material, a number of springs and dashpots may be needed and arranged in a propoer way.

Inclusion of more elements in a material model makes the practical use of the model more difficulty. A balance should be considered between accuracy and the practicality. One example is the Zener model [60]. Zener or standar solid model uses three elements as shown in Fig. 4. It consists of the Maxwell model in parallel with a spring. The stress-strain relation describing the material behavior is given as follows [61],

$$\sigma(t)+\tau_r \frac{d\sigma(t)}{dt} = E_\infty \varepsilon(t) + E_0 \tau_r \frac{d\varepsilon(t)}{dt} \tag{3}$$

Where $\tau_r = \mu/E_1$ is the relaxation time, μ is the dashpot viscosity, $E_0 = E_1 + E_2$ and $E_\infty = E_2$, E_1 and E_2 are spring constants.

The modified Zener model, where the fractional derivative is introduced, is more accurate in discribing a class of viscoelastic materials [60, 62-64]. The constitutive equation of the modified Zener model is [63],

$$\sigma(t)+\tau^\beta D^\beta \sigma(t) = E_\infty \varepsilon(t) + E_0 \tau^\beta D^\beta \varepsilon(t) \tag{4}$$

Where $D^\beta \sigma(t)$ and $D^\beta \varepsilon(t)$ are fractional derivative ($0 < \beta < 1$) of the stress and the strain, respectively. Note that if we set $\beta = 1$, the constitutive equation is reduced to Eq. (3).

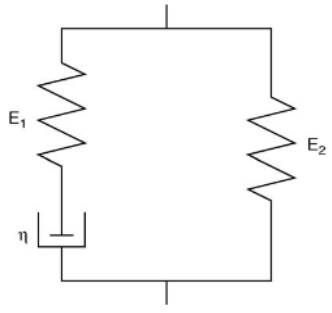

Fig. 4 The Zener model

In this thesis, we only consider the $\beta = 1$ case, the basic Zener model is thus used. The creep and relaxation functions are calculated from the constitutive equations, known as [61],

$$G(t) = E_\infty + (E_0 - E_\infty)\exp(-\frac{t}{\tau}) \tag{5}$$

$$J(t) = \frac{1}{E_\infty} + (\frac{1}{E_0} - \frac{1}{E_\infty})\exp(-\frac{E_\infty}{E_0}\frac{t}{\tau}) \tag{6}$$

Where $G(t)$ is the relaxation function which is used to describe the viscoelasticity of brain tissue, $J(t)$ is the creep function.

To obtain the stress-strain relation for brain tissues, experimental data are required. Creep and relaxtion data of brain tissues provided in [60] were used. Parameters of the material model are obtained by using the experiment data from [60] and the NonlinearFit command in Mathematica. The obtained parameters are listed in Table 1, and the relaxation behavior of the model is plotted in Fig. 5.

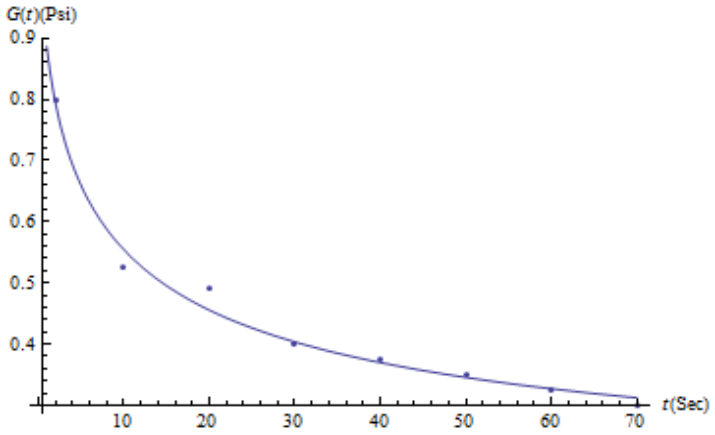

Fig. 5 Relaxation behaviour of brain tissue (reproduced from [60])

Table 1 Parameters in the viscoelastic mode of brain tissues

	E_∞ **(kPa)**	E_0 **(kPa)**	τ **(s)**	β
G	2.242	5.847	14.2235	1

In this thesis, commercial finite element software, ANSYS, was adopted in head injury analysis, and the element SOLID185 was used. The element has eight nodes and each node has three degrees of freedom. The software is not only able to simulate material behaviour such as plasticity, hyperelasticity, stress stiffening, creep, large strains, but also has the capability of predicting deformations of nearly incompressible elastoplastic materials, and fully incompressible hyperelastic mateirals [65].

In element SOLID185, the time-dependence viscoelasticity of a material is represented in terms of Prony series [65]:

$$G = G_0[\alpha_\infty^G + \sum_{i=1}^{n_G} \alpha_i^G \exp(-\frac{t}{\tau_i^G})] \tag{7}$$

$$K = K_0[\alpha_\infty^K + \sum_{i=1}^{n_K} \alpha_i^K \exp(-\frac{t}{\tau_i^K})] \tag{8}$$

Where:

G_∞, G_i = shear elastic moduli

K_∞, K_i = bulk elastic moduli

τ_i^G, τ_i^K = relaxation times for each Prony component

$\alpha_i^G = G_i / G_0$ is relative shear elastic moduli

$\alpha_i^K = K_i \big/ K_0$ is relative bulk elastic moduli

$G_0 = G_\infty + \sum_{i=1}^{n_G} G_i$ is instantaneous shear elastic moduli

$K_0 = K_\infty + \sum_{i=1}^{n_K} K_i$ is instantaneous bulk elastic moduli

n_G , n_K represent the number of Prony terms, which is also the number of parallel Maxwell models in the extended viscoelastic model.

The shear and bulk modulus are related to the Young's modulus by

$$G = \frac{E}{2(1+\upsilon)} \tag{9}$$

$$K = \frac{E}{3(1-2\upsilon)} \tag{10}$$

The viscoelastic behaviour of brain tissues are described by Eqs. (7), (8), (10), and the parameters in Table1.

2.4.3 Representation of Inhomogeneity of Head Tissues in Finite Element Model

Biological tissues are inherently inhomogeneous. How to represent inhomogeneity of head tissues is a challenging problem. Medical imaging provides a possible way to more accurately and more conveniently describe inhomogeneity of biological tissues. HU values in medical images, e.g. quantitative computed tomography (QCT), provide a realistic description of tissue inhomogeneity. Correlations exist between HU values and tissue ap-

parent density (density measured in fresh and wet conditions), and between tissue apparent density and tissue mechanical properties [66-68]. However, the specific correlationships are dependent on the used scanner, the X-ray energy level, and the tissues being scanned [69, 70]. The correlations established by Majumber et al. in [70] was adopted in this thesis. For the cortical bone of the skull, the HU values are in the range of [1255, 1955], while the apparent densities are in the range of [1.98, 2.27] (g/cm^3). For a linear correlation between HU and tissue apparent density, the two coefficients in the correlation can be determined by using the boundary conditions. The resulting linear correlation function is,

$$\rho_{cortical}(g/cm^3) = 0.000408163(HU + 1045) + 1.04898 \quad (11)$$

Similar procedure was used to determine the correlation function for the cancellous bone,

$$\rho_{cancellous}(g/cm^3) = 0.000476562(HU + 1045) + 0.633609 \quad (12)$$

Bone Young's modulus were correlated to bone apparent density by adopting the relations validated in [71, 72],

$$E_{cortical}(GPa) = 3.891(\rho_{cortical}(g/cm^3))^{2.39} \quad (13)$$

$$E_{cancellous}(GPa) = 2.0173(\rho_{cancellous}(g/cm^3))^{2.46} \quad (14)$$

For soft tissues such as the brain, there is no similar research reported in the literature. We assumed that there are similar correlations between soft tissue mass density and HU value, and between soft tissue mechanical properties and its mass density. The relationship between the apparent brain density and HU values was determined in the same way as for the bone.

$$\rho_{brain}(g/cm^3) = 0.000195312(HU + 1045) + 0.845313 \quad (15)$$

The Young's moduli of brain tissue used in the various numerical models presented in the literature spread over a range from 0.01 MPa to 5 MPa [45]. Herein, the average value (2.5 MPa) of these data is considered, we assume the Young's modulus of brain tissue in the current analysis is in the range of [2, 3] MPa. Similar to Eqs. (13) and (14), the power relationship is assumed to describe the relation between apparent density and Young's modulus for brain tissue. The same method as used to determine the coefficient of apparent density and HU values of bone is utilized. The relation between density and Young's modulus of brain tissue is expressed as,

$$E_{brain}(MPa) = 1.835(\rho_{brain}(g/cm^3))^{2.72} \quad (16)$$

The linear relationship between Poisson's ratio and mass density is assumed. The Poisson's ratio of skull bone is in the range of [0.2, 0.3], while the mass density is in the range of [1.5, 7.925]（g/cm^3）, so the coefficient can be determined as eq. (17). Similarly, the coefficient of relationship between Poisson's ratio of brain tissue and mass density can be determined. The obtained correlations for all head tissues are summarized in Table 2.

$$\upsilon = 0.045105\rho + 0.154895 \quad (17)$$

Table 2 Summary of functions for correlating head tissue mechanical properties to HU values

	The Skull		Brain tissue	CSF and others
	Cortical bone	**Cancellous bone**		
HU Range	$1255 < HU \le 1955$	$755 < HU \le 1255$	$55 < HU \le 755$	$0 < HU \le 55$
Apparent Density (g/cm^3)	$\rho = 0.000408163(HU+1045)+1.04898$	$\rho = 0.000476562(HU+1045)+0.633609$	$\rho = 0.000195312(HU+1045)+0.845313$	1.045
Young's Modulus	$E(GPa) = 3.891\rho^{2.39}$	$E(GPa) = 2.0173\rho^{2.46}$	$E(MPa) = 1.835\rho^{2.72}$	0.5(MPa)
Poisson's Ratio	$\upsilon = 0.045105\rho + 0.154895$		$\upsilon = 0.0098\rho + 0.48822$	0.4998

2.5 Material Mapping Procedure

Having established the correlations between tissue mechanical properties and HU values, the next step is to assign the mechanical properties to the FEHM. The public software BONEMAT has been widely used to assign material properties to the FE models [73-76]. In BONEMAT, Young's modulus is determined from HU values inside an element. For each element, the average value of the Yong's modulus over the element is calculated and assigned to the element. Therefore, variation of material properties over the problem domain is element-wise. The implementation of the method requires advanced programming or manual manipulations [77]. We introduced a different way for assigning material properties to FEHM created in ANSYS. The inhomogeneity of material properties over the FE model is introduced by using the temperature as an auxiliary parameter [72, 78]. Unlike the element-wise material distribution, as the temperature is an auxiliary parameter associated with element nodes in ANSYS, the variation of material properties over the

problem domain is node-wise, and therefore the newly introduced method is more accurately in representing material inhomogeneity. The apparent density is used as 'temperature' in ANSYS to assign Young's modulus at each node of the FEHM. This material mapping procedure can be divided into several sub-steps:

(1) Compute Young's modulus and apparent density corresponding to a given set of CT images using image processing command in MATLAB and the correlation equations in Table 2.

(2) Extract nodal coordinates of the FEHM by using ANSYS.

(3) Calculate material properties at the element nodes using HU values at the element nodes.

(4) Define Young's modulus and Poisson's ratio as dependent variables on apparent density using the 'temperature' field in ANSYS.

(5) Apply the nodal apparent mass densities obtained from CT slices to each corresponding node in the FEHM, Young's modulus at the nodes are assigned by $E(T)$ in ANSYS.

A sample CT slice and the corresponding mass distribution are shown in Fig. 6 to demonstrate the effectiveness of the mapping procedure. It can be seen from the figure that the inhomogeneity in mass distribution is fully captured by the mapping procedure. In the existing FEHMs, the cerebral cortex is represented by a smooth surface, which definitely affects the accuracy of strains. In our proposed FEHM, the non-smooth cerebral cortex is represented by the variation in material properties. Geometric fidelity to individual anthropometric parameters such as brain size, skull thickness, etc., is also well represented.

Differences in individual anthropometric parameters influence the distribution and magnitude of the maximum stress and strain inside the brain under similar impact [56, 79].

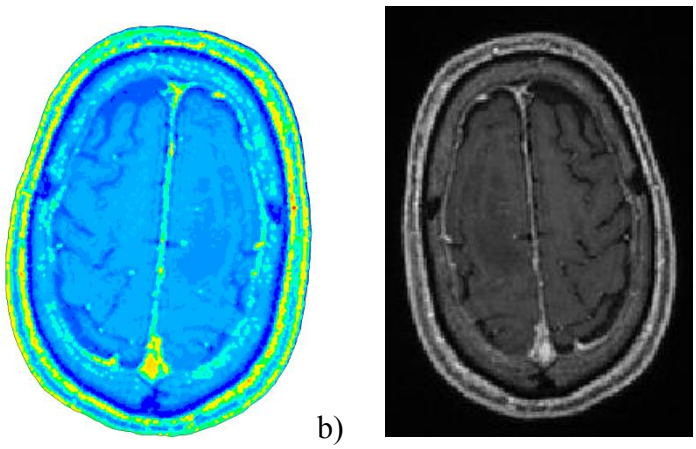

a) b)

Fig. 6 a) Mass density distribution; b) Sample CT slice

In the proposed FEHM, for the skull bones, the obtained mass density is in the range $[1491, 2273]$ (Kg/m^3), the Young's modulus obtained by the mapping procedure is in the range $[5, 23]$ (GPa). For the brain tissues, the density ranges from 1060 (Kg/m^3) to 1197 (Kg/m^3); the Young's modulus is in the range $[2.23, 3]$ (MPa). CSF layer has significant impact on the brain's mechanical response, for example, on the relative displacements between the skull and the brain. The relative displacements can cause contusions, intracerebral haematomas, and contrecoup lesion. In the proposed FEHM, the skull-brain interface is modeled also as solid elements but with a very small Young's modulus ($E = 0.5(MPa)$). Therefore, the relative motion between the skull and the brain is characterized by large displacements the CSF undergoes during an impact process. Representation of material inhomogeneity is significantly improved by the above

mapping procedure. Sample distributions of mass density and Young's modulus in the middle sagittal section obtained the mapping procedure are shown in Fig. 7.

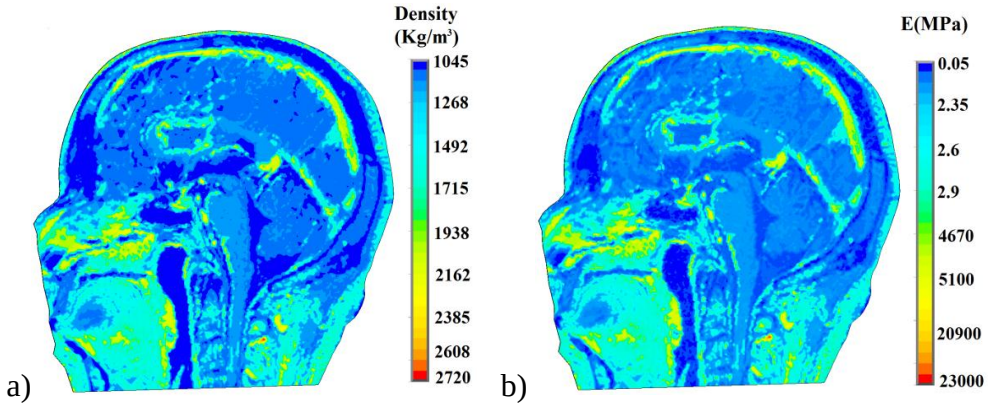

Fig. 7 Mechanical properties obtained by the mapping procedure a) tissue density; b) Young's modulus

2.6 Convergence Study

In the developed FEHM, inhomogeneous material properties are assigned to the corresponding element nodes. The accuracy of the developed FEHM is obviously dependent on the number of FE nodes. The convergence of the developed FEHM may also be different from that of conventional FEHMs due to the inclusion of inhomogeneous material model. Thus, the convergence of the developed FEHM was studied. The study included two aspects, i.e., the effect of mesh density and the effect of time-step length on the convergence of the developed FEHM. The effects of the two factors were measured in terms of variations in the maximum von Mises strain and the maximum intracranial pressure.

Due to the limitation of available computing capacity, a two-dimensional (2D) FEHM was used in the convergence study. The 2D FEHM was constructed from a CT slice that is 33 mm away from the top of head. A step impulse having duration of 5 ms was used as

input, and the responses of the FEHM to the impulse in the first 10 ms were studied, as it was found that the maximum intracranial von Mises strain and the maximum intracranial pressure occurred in the first 10 ms after the application of the step impulse. FEHMs with different number of elements (element nodes) were compared to study the influence of mesh density. Results show that the number of nodes has effect on the convergence of the developed FEHM. First, it was found that the material mapping results are directly related to mesh density. The FEHM with higher mesh density has a much higher fidelity in representing the anatomic components of the head as shown in Fig. 8.

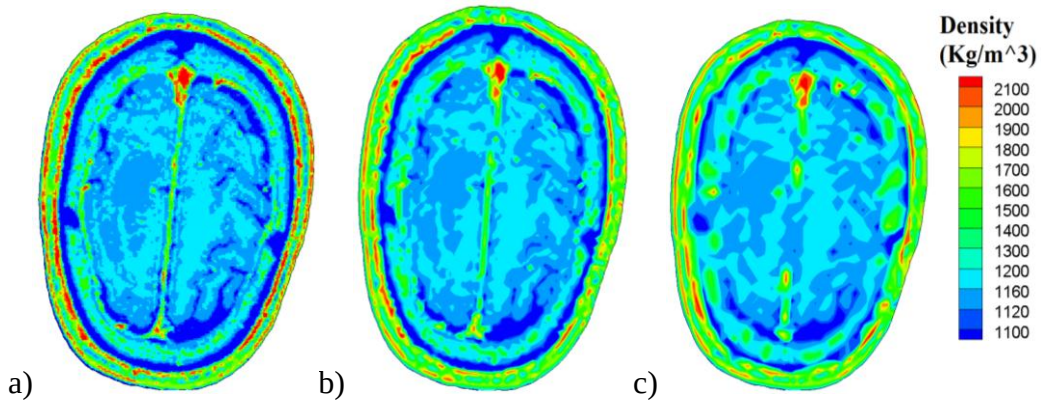

Fig. 8 Apparent density distributions in FEHM with a) fine mesh density; b) medium mesh density; and c) coarse mesh density

Second, it was observed that the values of the maximum von Mises strain and the maximum intracranial pressure approach constants with increasing number of nodes see Figs. 9 and 10. When the number of nodes reached approximately 25000, the values of the two parameters were almost constant. The FE solutions are mesh - independent when the number of nodes is larger than this threshold.

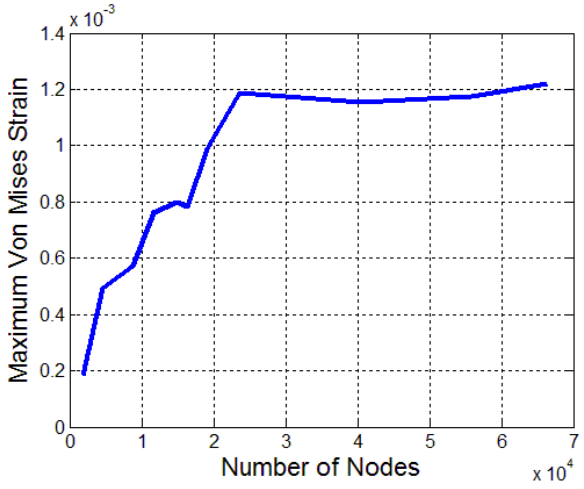

Fig. 9 Effects of mesh density on maximum von Mises strain

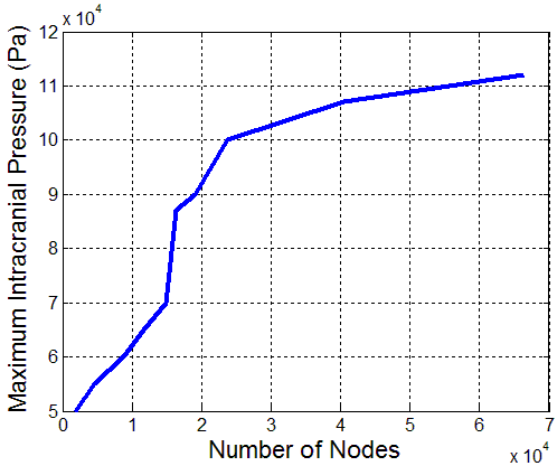

Fig. 10 Effects of mesh density on maximum intracranial pressure

Influences of the length of time step were also investigated. The applied impact duration also has duration of 5 ms. FE solutions obtained with different lengths of time step were compared. Results showed that the maximum von Mises strain and the maximum intracranial pressure changed considerably with different lengths of time step. When the length of time step was reduced to approximately 0.125 ms, the values of the von Mises strain were almost constant. The convergences of the maximum intracranial von Mises strain and the maximum intracranial pressure are displayed in Figs. 11 and 12.

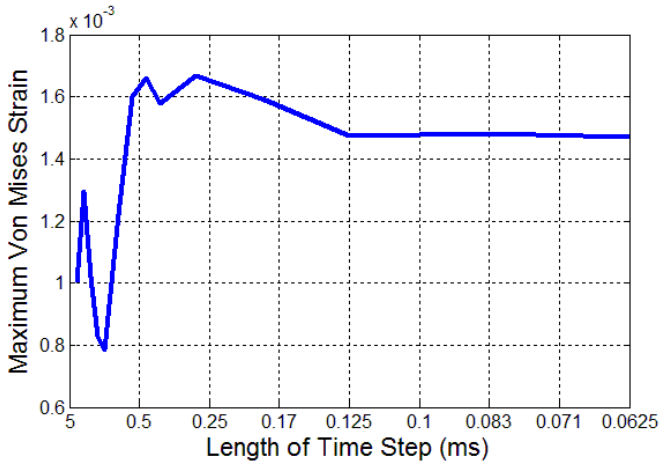

Fig. 11 Effects of time step length on maximum von Mises strain

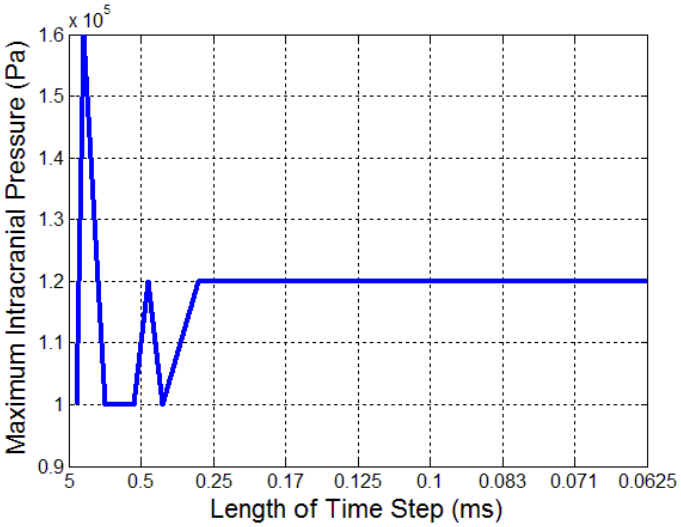

Fig. 12 Effects of time steps on maximum intracranial pressure

Variations of intracranial pressure along the anteroposterior cord shown in Fig. 13 a) at different time instants are displayed in Figs. 13 b) – e).

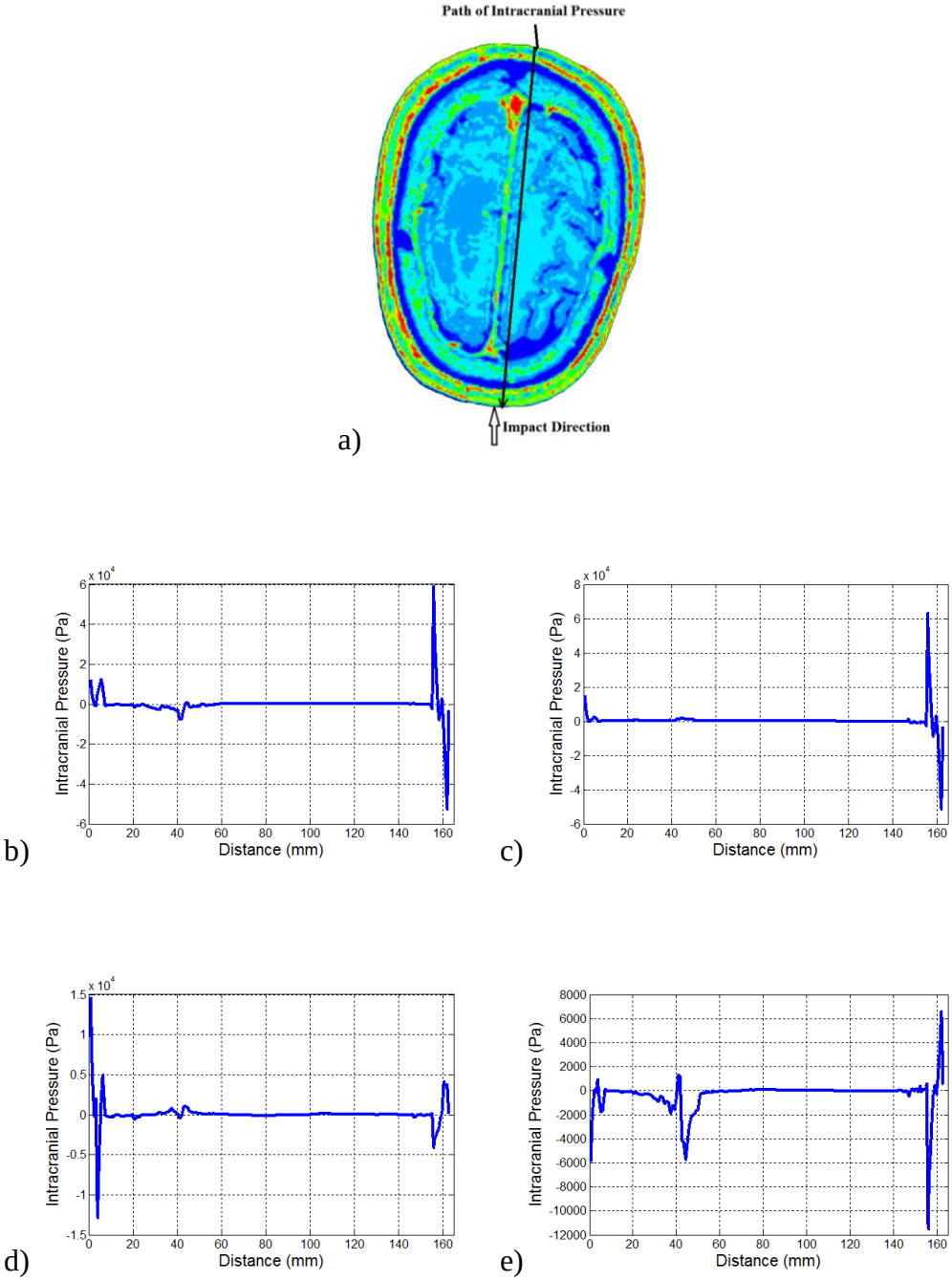

Fig. 13 Intracranial pressure distributions at four time instances a) path of pressure; b) at 3 ms; c) 5 ms; d) 7 ms; e) 10 ms

2.7 Model Validation against Experimental Data

The proposed FEHM was validated against experimental data reported in the literature. The experiment results of cadaver impact test conducted by Nahum et al. [30] was used in the validation. In the experiment, a cadaver was seated and impacted on the forehead. To mimic real-world impact, the head was positioned forward so that the Frankfort anatomical plane was inclined 45^o to the horizontal (Fig. 14). Intracranial pressures were recorded by pressure transducers at five locations, i.e. the location behind the frontal bone and adjacent to the impact area (coup site), the location immediately posterior and superior to the coronal and squamosal suture in the parietal area (parietal site), the location inferior to the lambdoidal suture in the occipital bone (one in each side) (occipital site 1 and 2), and the posterior fossa in the occipital area (contrecoup site).

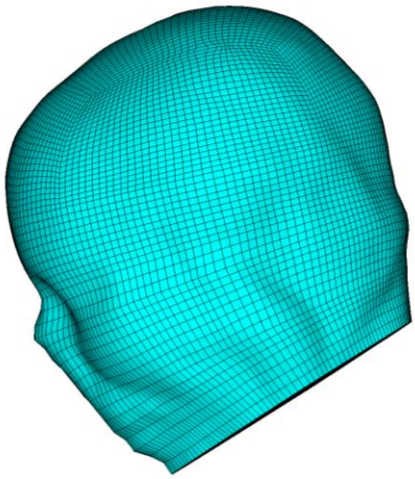

Fig. 14 FEHM positioned in a similar way as in Nahum's impact test

To numerically reproduce Nahum's experiment, the impact force was estimated from the measured coup site pressure in Nahum's report [30], see Fig. 15. The impact force was applied to the mid-frontal area of the head model in the horizontal direction over an area

of 1,556 mm^2. Similar impact force was used by Chen et al. in their FEHM [38]. In the existing FEHMs, free boundary conditions are applied by assuming that the head-neck joint has no effect on the dynamic behaviour of the head if the impact is only exerted for a very short time (<6 ms) [50]. Chen et al. [38] considered two extreme boundary conditions, i.e., free and fixed boundary conditions, to obtain the upper and lower bounds of the finite element solutions. In our study, the bottom of the neck was fixed in the finite element simulation.

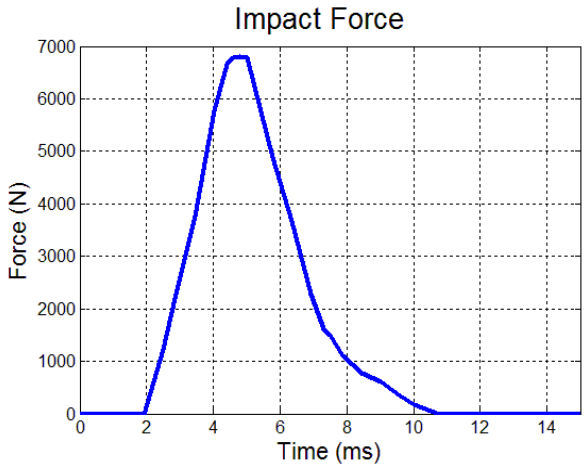

Fig. 15 Impact force retrieved from Nahum's cadaveric experiment

The mass of the head was calculated as 4.6025 kg, which is around the average weight of adult head cut off around vertebra C3. Pressure time histories obtained by the proposed FEHM at the five sites, i.e., coup, contrecoup, parietal site and occipital 1 and 2, together with the intracranial pressures measured in Nahum's test, are plotted in Figs. 16 - 19. Numerical results from [38] using the free boundary conditions, which provides the upper bound of the results, are also shown in the figures for comparison.

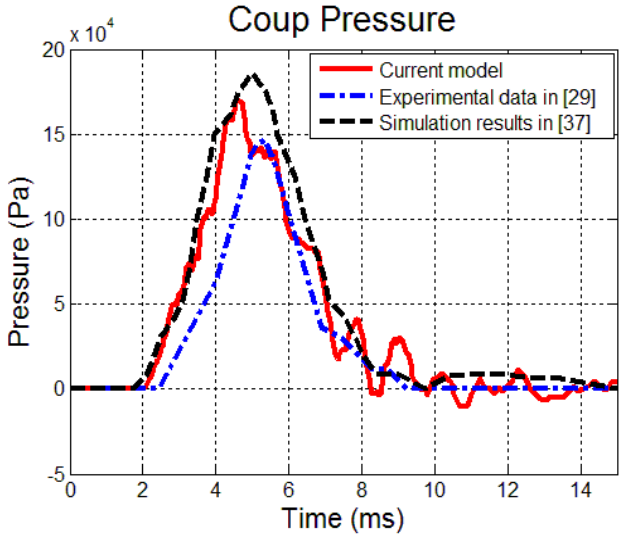

Fig. 16 Comparison of coup pressure

The intracranial pressure obtained by the proposed finite element head model is similar to the experimental data and to Chen's FE results. However, oscillations are found in the numerical results. There are several possible reasons. The decay time of the viscoelastic material model is 14.2235 s, while the impact process is about 15 ms. Therefore, the viscosity of brain tissues did not play a role in damping out the vibrations. For the proposed FEHM, material mapping results are obviously related to mesh density [74]. A finer mesh will yield a higher resolution in the material distribution [77]. To reveal detailed anatomic structures in head tissues, a very fine FE mesh must be used. However, the computational time required to run the simulation will be very long (about a few days with the available desktop computer). In order to reduce the computation time, the minimum edge length of elements was set to 2mm the regions where higher accuracy is desired, e.g., in the brain tissues. Coarser FE meshes were used in other less important regions. At the contrecoup site, the minimum edge length of elements was set to 4mm, which seems not adequate for capturing the reflected mechanical wave, as can be seen from Fig. 17. This deficiency can

be eliminated by further refining the mesh around the posterior fossa region, if more powerful computer is available in the future.

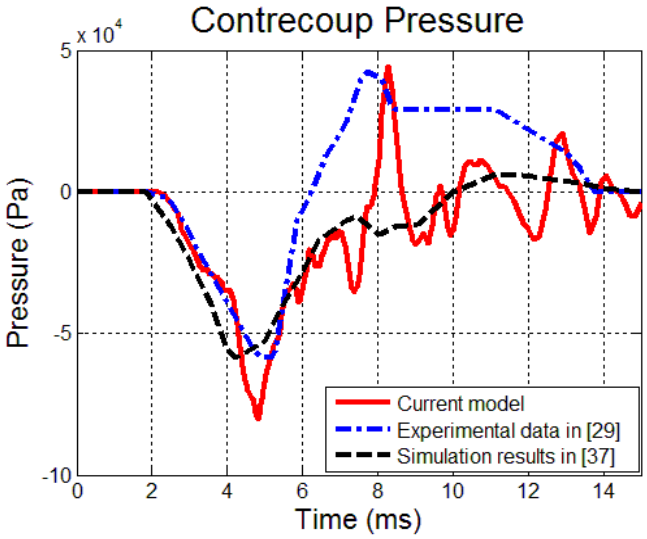

Fig. 17 Comparison of contrecoup pressure

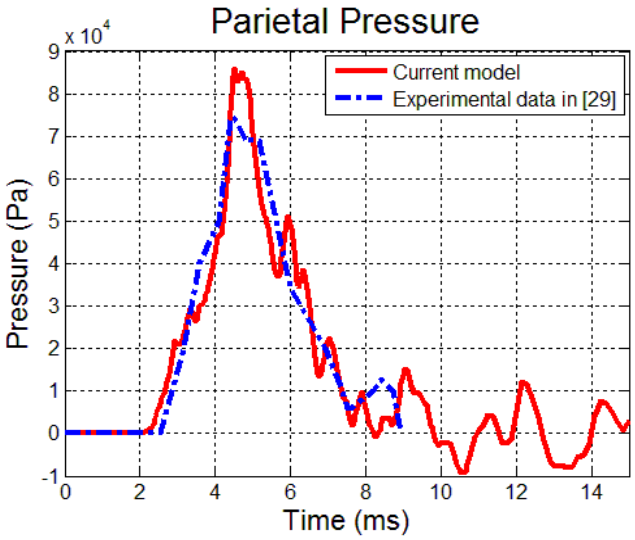

Fig. 18 Comparison of parietal pressure

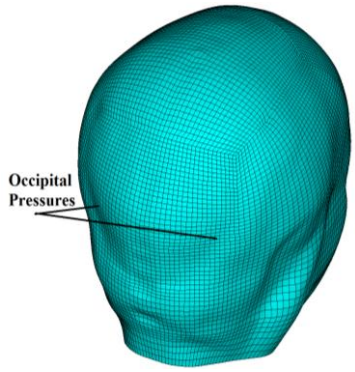

a)

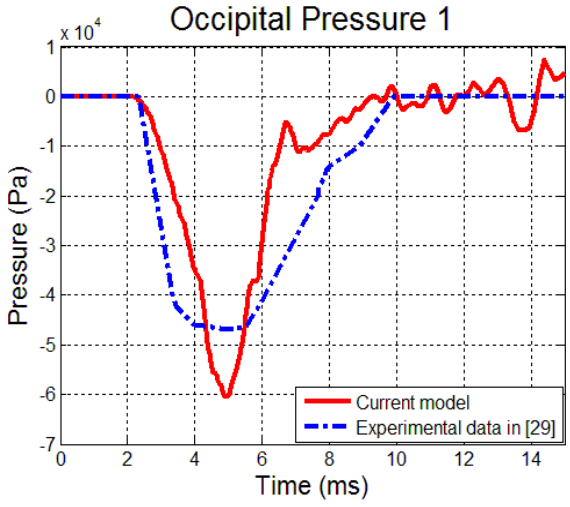

b)

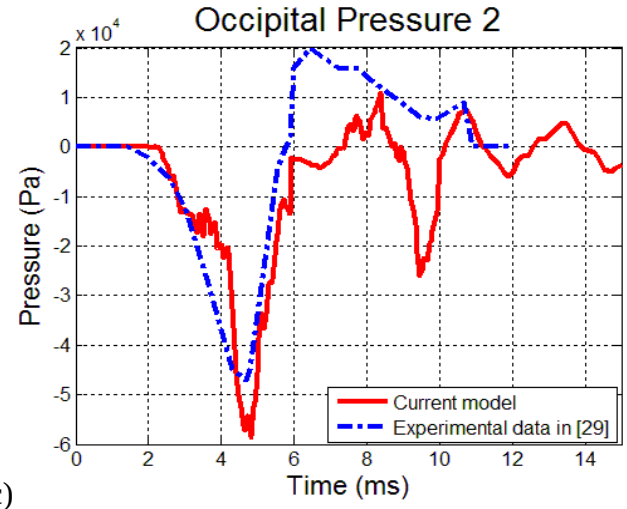

c)

Fig. 19 a) locations where occipital pressure were measured and calculated; b) and c) occipital pressure at location 1 and 2, and their comparison with experimental results

2.8 Prediction of Brain Injuries Caused by Angular Acceleration Impulse

Angular acceleration with or without direct impact is an important mechanism in head injuries. The large shear strain and tensile strain generated by rotational impulse may cause cerebral contusion such as DAI. The mechanism can be demonstrated by an analogy of bowl of porridge (Fig. 20). When the bowl is given a rapid rotation (angular acceleration), a part of the porridge adjacent to the bowl will tend to move with the bowl and the center will tend to remain stationary. This relative motion caused by shear stresses can cause severe injury to the brain tissues [80].

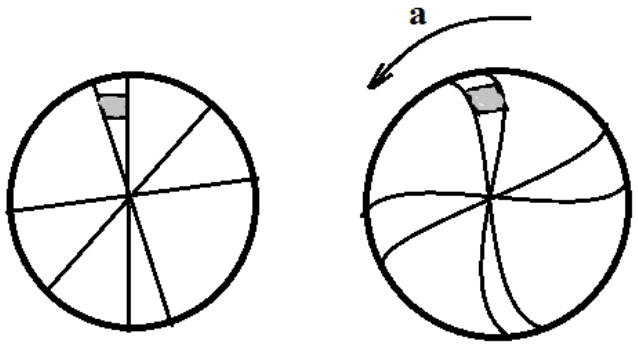

Fig. 20 Shear strains produced by the angular acceleration of bowl

In the proposed FEHM, the CSF layer which is the main cause for the large relative motion between the skull and the brain is modeled as solid elements with lower shear modulus. In reality, because of its fluid-like property, CSF is not able to sustain any substantial shear stresses. A large relative motion will be induced by an angular acceleration. The ability of the developed FEHM in capturing the large shear strains induced by a rotation impulse is important for predicting brain injuries and thus must be examined. A special

loading condition where the head sustains pure rotation acceleration was investigated. The step angular acceleration impulse is shown in Fig. 21. The mechanical responses of the head in the first 10 ms were obtained.

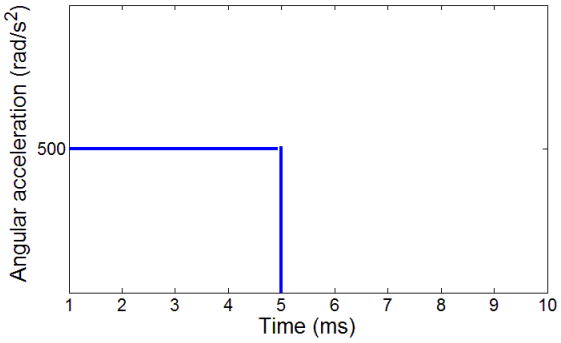

Fig. 21 Angular acceleration impulse for the head model

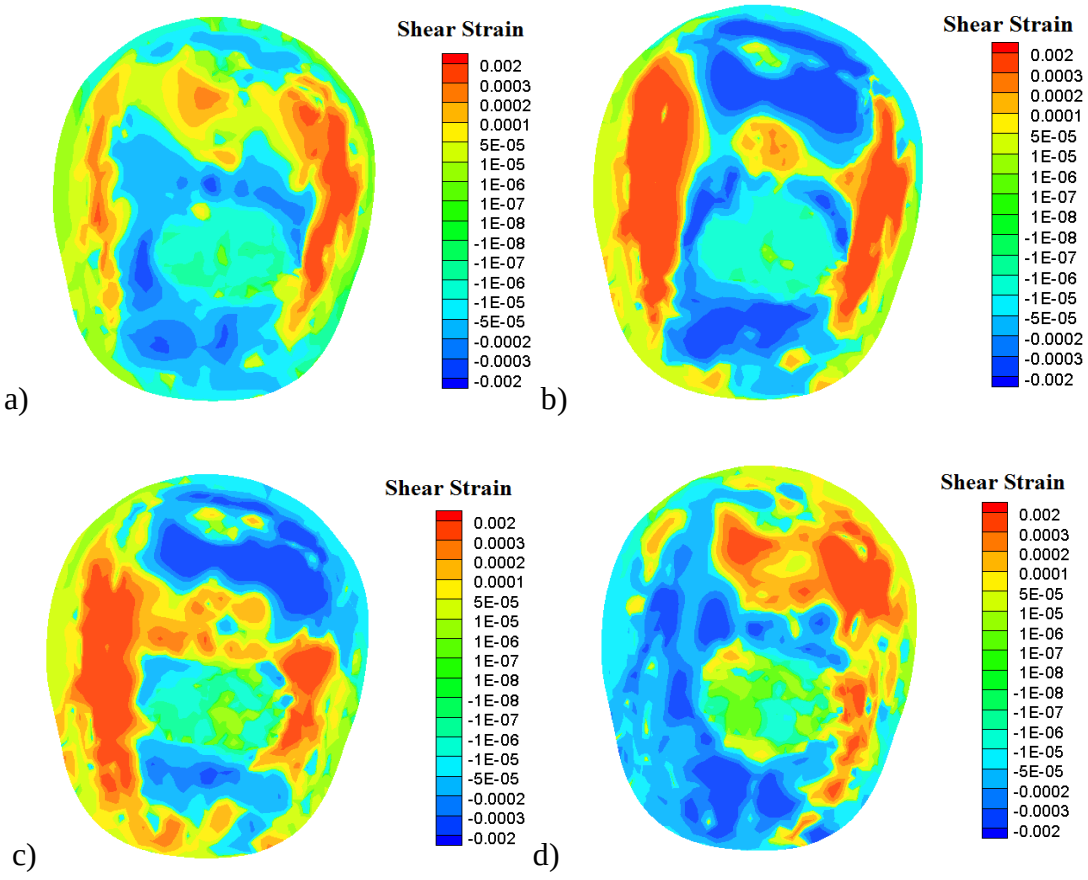

Fig. 22 Shear strain distributions at a) T= 1ms, b) T=2 ms c) T= 6 ms d) T= 9 ms

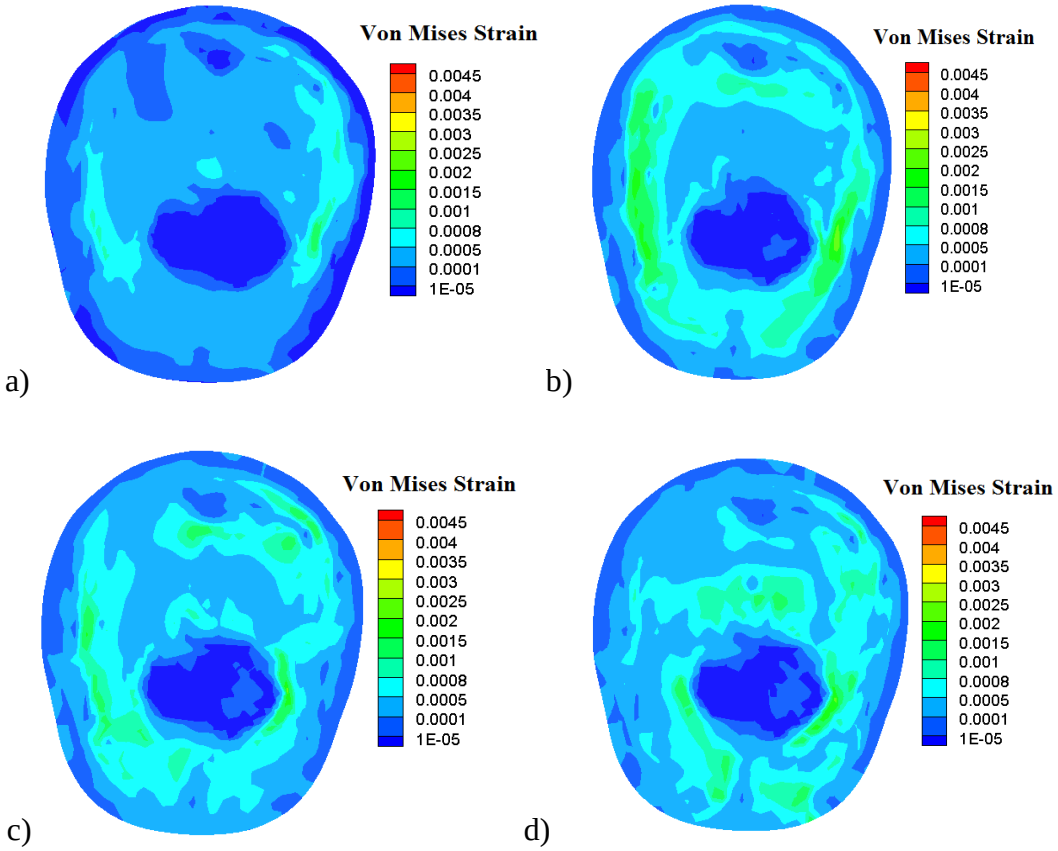

Fig. 23 von Mises strain distributions at a) t= 1 ms; b) t=2 ms; c) t= 6 ms; d) t= 9 ms

The shear strains and von Mises Strains obtained at different time instants after the application of the impulse are shown in Figs. 22, and 23. From the above figures, it can be observed that the CSF layer indeed experienced larger shear strains as expected. Larger relative displacements between the skull and the brain are introduced, which is a high risk to the bridging blood vessels connecting the skull and the brain. It was found from the above simulation large strains exist around the ventricle, which may induce diffused axonal injury. This finding is consistent with anatomic results of Stage 2 DAI, which usually occurs at the corpus callosum and around the ventricles. Brain tissues around the ventricles tend to rotate when they are subjected to a sudden angular acceleration while the

ventricle in the middle of the brain tends to keep stationary. The irregular surfaces of the ventricles act as a barrier for the brain to freely rotate around the ventricle. The large shear strains contribute to the rupture of blood vessels and lead to brain injuries.

2.9 Investigation of Effects of Homogeneous vs. Inhomogeneous Material Model

Due to the lack of direct experimental data on inhomogeneous material model, homogeneous material models are adopted in all existing FEHMs. The differences between the developed FEHM with inhomogeneous material properties and conventional FEHM with homogeneous material properties were investigated.

The same step impact impulse as shown in Fig. 24 and the same boundary conditions were used in the investigation to compare the two different FEHMs. The FEHM assigned with homogenous material property is shown in Fig. 25. The model with inhomogeneous material property is same as Fig. 8a. In order to compare with results from the inhomogeneous FEHM in a reasonable way, material properties of the homogeneous FEHM were taken as the average value of the corresponding head tissues of the inhomogeneous model, see Table 3. For instance, the Young's modulus of cancellous bone in the inhomogeneous material model is in the range of [5.393, 7.93] GPa, the Young's modulus of cancellous bone in the homogeneous model is taken as 6.66 GPa. The rest parameters are assigned in the same way. The viscoelasticity model same as in the inhomogeneous material model is used in the homogeneous material model.

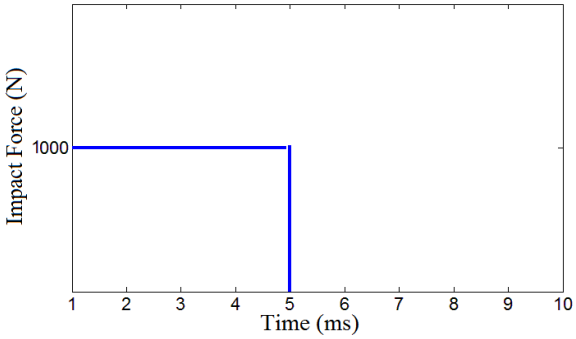

Fig. 24 Impact force

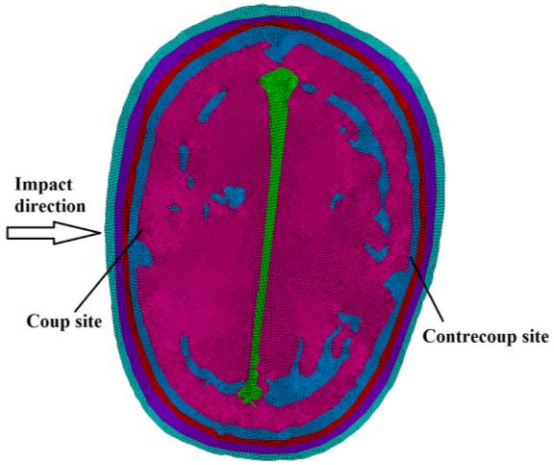

Fig. 25 FE model assigned with homogeneous material

Table 3 Homogeneous material properties of head tissues

		E (MPa)	Density (kg / m^3)	Poisson's ratio
Skull bone	**Diploe**	6660	1618	0.22
	Inner/outer table	15000	2131	0.22
Brain		Viscoelastic material	1128	0.4996
CSF		0.5	1045	0.489
Dura Matter		30	1130	0.45

The von Mises strain distributions at two different time instants are plotted in Fig. 26. Relatively larger strains can be observed in the inhomogeneous model, especially around the center of the brain. At t = 1.6 ms, the von Mises strain of the inhomogeneous model in the middle part of falx is approximately 0.007, at the same location of the homogeneous model is about 0.003. The maximum von Mises strain predicted by the inhomogeneous model is almost 2 times larger than that of the homogeneous model, while the maximum shear strain in the inhomogeneous model is 1.3 times larger than the homogeneous case at t = 5 ms (Table 4). The inhomogeneous material model predicts higher intracranial strains, which is probably a more realistic prediction.

Coup-contrecoup injury is a common brain injury during the impact. How the inhomogeneous material model would predict the contrecoup injury is of great practical significance. The von Mises strain time histories obtained by the homogeneous and inhomogeneous model at the contrecoup site are plotted in Fig. 27. From the figure, we can see the opposite impact site of inhomogeneous material model experienced larger strains. The maximum von Mises strain of the inhomogeneous material model was about 4.9E-5 and occurred at 2.4 ms, while the maximum von Mises strain of the homogeneous model was 0.8E-5 and appeared at 2 ms. For a brain injury based on maximum von Mises strain, the homogeneous material model would provide a more conservative prediction.

Results showed that the inhomogeneity of the brain influenced the dynamic response of brain. From the viewpoint of wave propagation, due to the complex structure (represented by different material distribution), successive reflections and refractions of the local waves at the interfaces may lead to dispersion, strengthening/attenuation of the global

wave field which are difficult to quantify. The small – scale changes in the inhomogeneous material's microstructure can have major effects in its macro – scale behavior (dynamic behavior of brain). In the current test, the homogeneous material model underestimates the maximum von Mises strain during the impact process, thus the predictive ability of the FEHM using homogeneous material model is discounted. The injury criterion based on the inhomogeneous material model need to be further investigated.

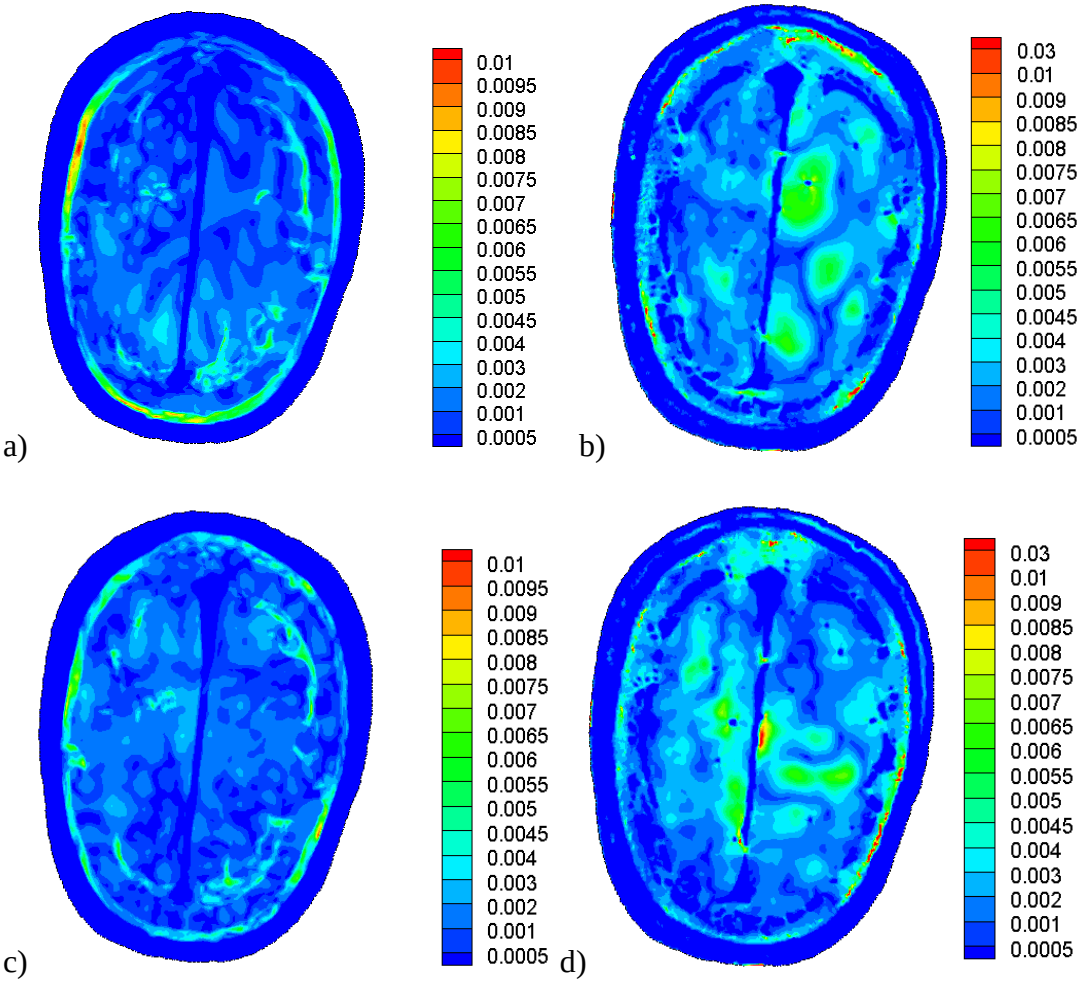

Fig. 26 von Mises strain distribution of a) homogeneous model at t= 1.6 ms; b) inhomogeneous model at t= 1.6ms; c) homogeneous model at t= 9.5 ms; d) inhomogeneous model at t= 9.5 ms

Table 4 Comparison of stress/strains between homogeneous and inhomogeneous model at t = 5 ms

	Homogeneous model	**Inhomogeneous model**
Maximum von mises strain	0.0088	0.026
Maximum von mises stress (MPa)	1.6	2.37
Maximum shear strain	0.0074	0.017
Maximum shear stress (MPa)	0.41	1.03

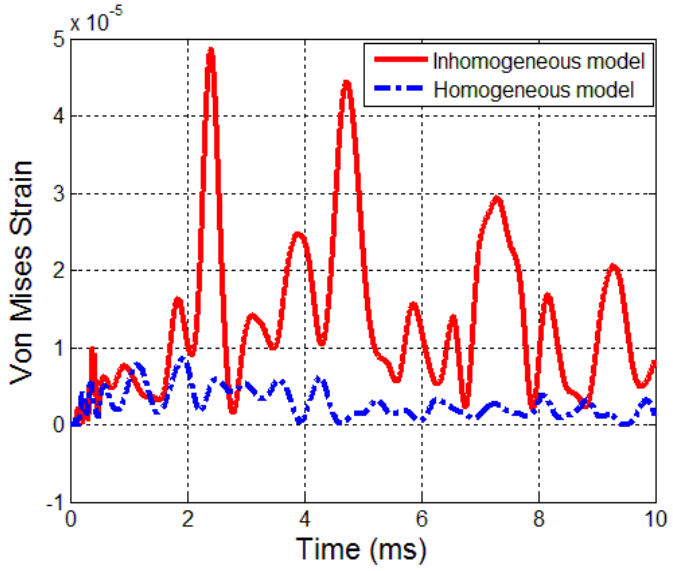

Fig. 27 Comparison of von Mises strain distribution at the contrecoup site

2.10 Conclusions

In this chapter, a new FEHM was developed to improve material biofidelity. Assignment of inhomogeneous material properties in the head model was implemented by using HU values of the medical images. This inhomogeneous material model was demonstrated more loyal to the real material distribution of head tissues than a homogeneous model. Based on the obtained investigation results, the following conclusions can be drawn:

1) The procedure of constructing FEHM with inhomogeneous material properties was established. Relationships between HU values of CT images and mechanical parameters of head model were set up. Different anatomic components in the head were represented by different material properties inside the FE model. The FEHM with inhomogeneous material model provides an alternative way to those proposed in the literature, which has the advantages of simpler geometric model and higher quality of FE mesh.
2) The FEHM was validated with experiment data of intracranial pressure available in the literature. Good agreements were observed in general. However, oscillations were found at the contrecoup site of predicted mechanical responses by the developed FEHM. A coarse mesh that was not able to capture the reflection of the waves around this site was one possible reason. The accuracy of the current head model was affected by the mesh density.
3) The thin CSF layer was modeled by solid elements with soft material property. The ability of the current model in simulating the large strain especially the shear strain was demonstrated. In the predicted mechanical responses to an angular impact, large strains/stresses were observed in the CSF layer. These regions thus have higher risk of injury.
4) The inhomogeneous material model has a great influence on the mechanical responses of the head model. The brain simulated by the inhomogeneous material model experienced larger strain than the homogeneous model. The inhomogeneous material model predicted much higher maximum peak von Mises strain, and is thus more sen-

sitive to head injury than a homogeneous model. A FEHM with the homogeneous material model may underestimate the maximum peak von Mises strain inside the cranium and thus the predictive ability of a homogeneous material model is discounted.

Chapter 3

Image-Based Virtual Helmet Design

3.1 Introduction

There are two major head injury modes under impact, skull fracture and focal brain injuries (contusions and haematomas). High localised compressive stresses induced in sports, military action, factory and traffic accidents by impacts are the main cause of brain injuries. A helmet is considered an effective protection device to reduce the risk of head and brain injuries. The effectiveness of helmet in protecting the head from accident impacts is well documented. By wearing helmets, head and brain injuries is reduced by about 70 to 88% and facial and mid-face injuries by 65% [81]. The mechanical mechanism of protection provided by helmet is based on mechanical energy absorption by the helmet materials. Main components of a helmet include the foam liner and the stiff shell. The functionality of the foam is to absorb most of the impact energy and spread the rest of the impact force from the rigid shell to a larger contact area of the skull. The risk of brain damage is thus considerably decreased. When the foam is deformed by compression, it reduces the acceleration induced by the impact. The hard shell layer is used to resist foreign object

from penetrating the head and resulting in skull damage. Helmets made of composite shell have shown to be more advantageous than traditional ones made of steel and thermoplastic shells, in terms of helmet weight and impact resistance [82, 83]. Composite materials not only have desired mechanical properties, but also offer greater flexibility in design.

A well designed helmet should be able to absorb as much mechanical energy as possible and to distribute the rest of impact energy to the largest possible contact area between the liner and the head. The liner part of the helmet plays a critical role in the energy absorption and the stiff shell layer acts as a protector from penetration. Therefore, influences of changing liner parameters and the stiffness of the shell on the dynamic behaviours of a helmet under impact must be investigated. Parametric studies were conducted to find out how changed parameters of the liner and the shell would affect the dynamic behaviour of the helmet-head system.

3.2 Construction of Helmet Geometric Model

The inner surface of the helmet was extruded from the surface of the skull to make the liner part closely contact to the head surface. An 8 nodes brick element solid 185 was used to model the elasto-plastic material properties of foam. The outside surface of the helmet was composed of five layers of composite material which is represented by Solid46 elements. Contact elements were defined between the head and the helmet. The developed helmet-head system is showed in Fig. 28. The FEHM developed in Chapter 2 was used in the helmet-head system.

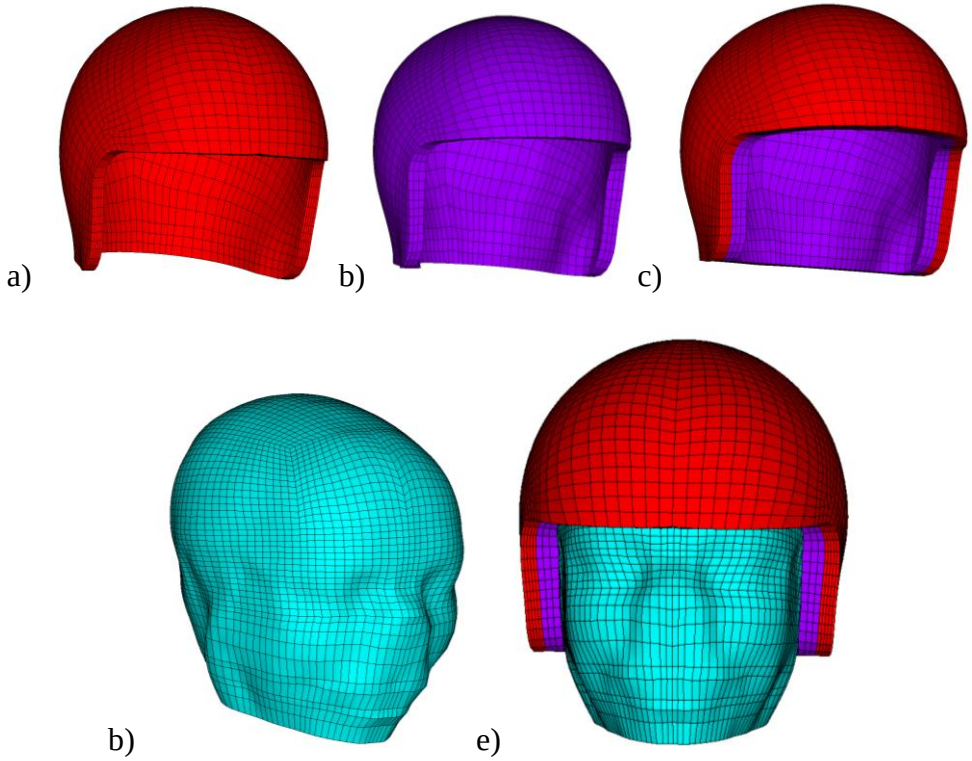

Fig. 28 a) Composite shell; b) liner component; c) helmet model; d) head model; e) helmet-head system

3.3 Material properties of helmet components

3.3.1 Composite shell

With the rapid advances in material science and technology, composite materials have more and more engineering applications such as aerospace, automobile and sports. The commonly used type of composite materials is laminate, which is made by stacking a number of thin layers of fibres and matrix and consolidating them into the desire thickness. Different ply angles of the fibres would result in different stiffness of laminate. Therefore, composite materials can be designed to have the desired strength. In our re-

search, we considered three types of composite materials that are commonly used in manufacturing helmets. The mechanical properties of the three composites are listed in Table 5. Parametric studies were conducted to study the influences of stiffness of composite materials on the dynamic responses of the helmet-head system. As there are many choices in laminate angles, we only considered the orthogonal layout, i.e., [0/90/0/90/0].

Table 5 Mechanical properties of fibre reinforced composites [83]

	Carbon fabric reinforced polyester	**Glass fabric reinforced polyester**	**Kevlar fabric reinforced polyester**
Density (Kg/m^3 **)**	1800	2000	1650
E_{11} **(GPa)**	61.3	19.7	32.4
E_{22} **(GPa)**	61.3	19.7	32.4
E_{33} **(GPa)**	10	9.5	9.5
υ_{12}	0.0313	0.1	0.0484
υ_{13}	0.4	0.25	0.3
υ_{23}	0.4	0.25	0.3
G_{12} **(GPa)**	2.77	3.1	1.8
G_{13} **(GPa)**	2	2.5	1.35
G_{23} **(GPa)**	2	2.5	1.35

3.3.2 Foam material properties

The liner is mainly made of polystyrene foam, which serves as the energy absorbing component. The foam is a non-linear viscoelastic material. The constitutive law for foam material is based on experiments at various rates and includes the effects of foam com-

pressibility. Fig. 29 shows a typical stress-strain relation of foam material. The stress-strain relation is characterised by three stages: (1) a short linear elastic stage at low stress level; (2) a plateau stage, -- the longer the plateau, the more energy it can absorb without increasing the stress; and (3) the final stage, which consists of foam densification. The mechanical behaviour of a foam material is related to its density. The area under the stress-strain curve gives the energy absorbed by the foam. The stiffness of a foam material increases with its density (Fig. 30) [84].

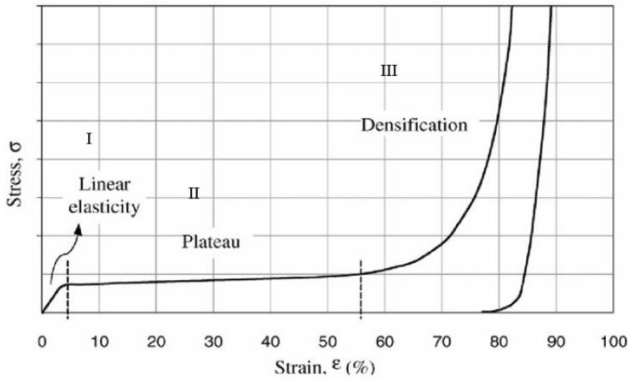

Fig. 29 Classical stress-strain relation of foam material under uniaxial compression [85]

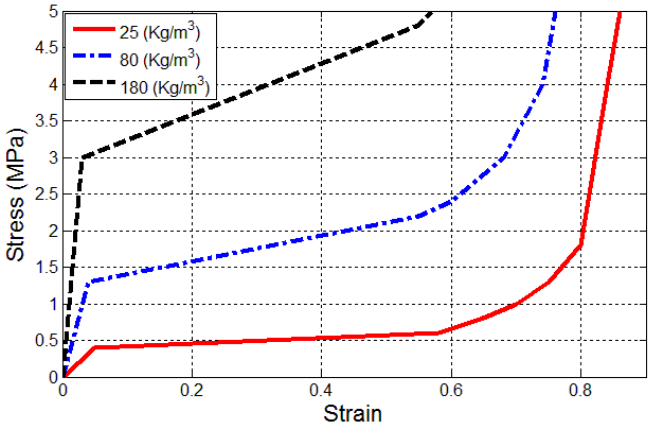

Fig. 30 Compressive behaviour of polystyrene foam with different density [84]

3.4 The protection role of helmet

FEHMs with and without helmet were studied and compared to see how a helmet would protect the head from an impact. A triangular impulse having duration of 1 ms was applied to both helmeted head model and head model without helmet. Mechanical responses of the head in the first 1.5 ms were studied. Dynamical responses of the head with and without a helmet were compared in terms of coup and contrecoup pressure, as they are related to coup-contrecoup injuries. From the results displayed in Figs. 31 and 32, we can see that wearing a helmet significantly decreases intracranial pressure of the head. Without helmet, the maximum intracranial pressure at the coup side is about 0.03 MPa and occurring at 1.1 ms, while the maximum intracranial pressure of the helmeted head is about 0.01 MPa and appearing at 0.8 ms. The maximum contrecoup pressure for the head without helmet is 0.09 MPa occurring at 1 ms, while for the helmeted head it is 0.015 MPa occurring at 1.25 ms. The mechanical energy transferred to the head is greatly decreased by the helmet. Compared to the intracranial pressure value of the helmeted head, the intracranial pressure in the head directly exposed to the impact is much higher and thus the head has a much higher chance of injury. It was observed from simulations that the contrecoup pressure was even higher than the coup pressure without the helmet. This is consistent with clinical observations and suggests that contrecoup injury can be even more severe than the coup injury in an impact. In a closed head injury, the skull is abruptly stopped; the in - vivo CSF which is denser than the in vivo brain moves toward the site of skull impact, while the brain is lagged. If the extent of deceleration produces sufficient force to cause displacement of the brain relative to the skull, the initial movement of the

brain will be in a direction away from the location of the skull impact, resulting in initial impact of the brain parenchyma with the internal surface of the skull at the contrecoup location. This initial displacement of the brain toward the contrecoup location results in the contrecoup injury being of greater severity than the coup injury [86].

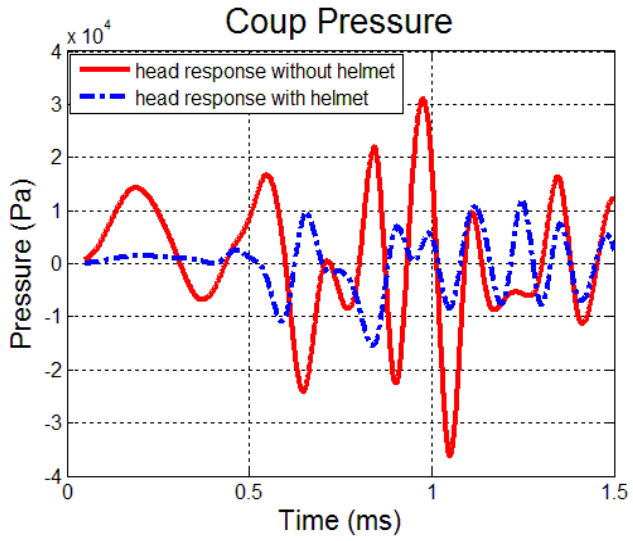

Fig. 31 Comparison of coup pressure between head model with and without helmet

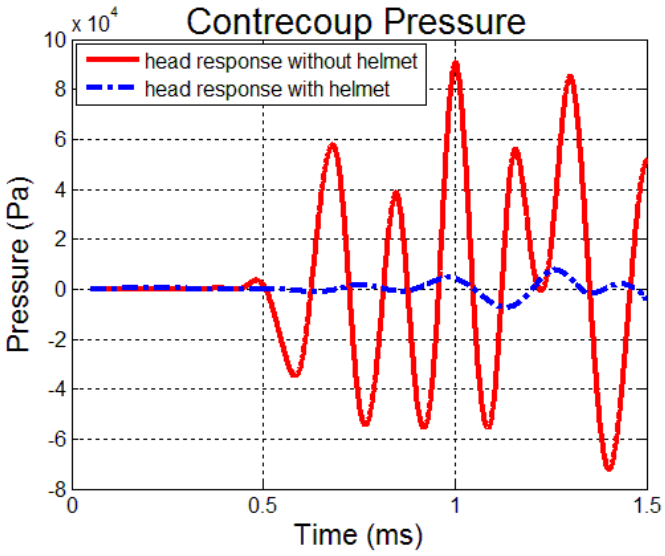

Fig. 32 Comparison of contrecoup pressure between head model with and without helmet

3.5 Influence of composite shell stiffness

Three different composite materials which are widely used in the fabrication of helmets were employed to investigate the influences of composite shell stiffness. The composite shell of the helmet was divided into five layers. Due to the limited composite material models available in FE analysis software, each layer is assigned with homogeneous and orthotropic material property (Table 5). A triangular impulse with duration of 1 ms was applied. The responses of the helmet-head system in the first 1.5 ms were studied. To reveal the effects of the stiffness of composite shell on the dynamic responses of the helmet-head system, pressure at coup and contrecoup side, where brain injuries most often occurred, were investigated (Fig. 33, Fig. 34). No significant difference was introduced in the pressure at either the coup side or the contrecoup side by the different shell stiffness. The resultant maximum von Mises strains in the head for these three cases are also similar to each other (Table 6). There are two possible reasons leading to this phenomenon.

1) The differences in the impact performance of the composite helmet are attributed to the values of shear strength and G_{12} shear modulus of the lamina used. The in-plane moduli of elasticity and normal strength do not have significant direct effect on the performance of helmet [83]. For the three examined cases of material combination, the shear moduli of the composites are very close to each other (see Table 5). The major differences in three composites are from the in-plane Young's moduli (E_{11} and E_{22}).
2) Microscopic failure of composite material in impact was not considered. However, the advantage of fibre reinforced materials is to absorb mechanical energy by allow-

ing a certain level of microscopic failure such as fibre rupture and matrix cracking. Under a high energy impact, rupture of fibres and cracking of matrix in composite material is able to absorb a large portion of the mechanical energy. However, the above mechanism of energy absorption was not considered in the current analysis.

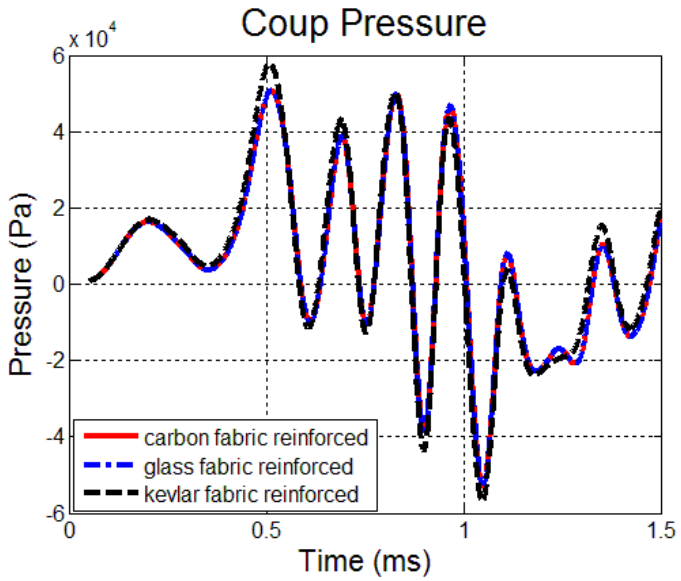

Fig. 33 Coup pressure time histories with different composite shell stiffness

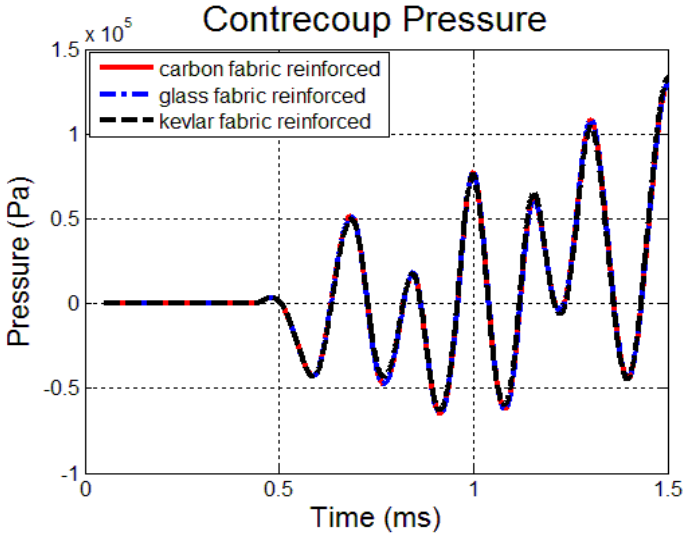

Fig. 34 Contrecoup pressure time histories with different composite shell stiffness

Table 6 Comparison of maximum von Mises strains in the brain when different composites are used

	Carbon fabric reinforced polyester	**Glass fabric reinforced polyester**	**Kevlar fabric reinforced polyester**
Maximum intracranial von Mises strain	0.0292	0.033	0.0341

3.6 Influence of foam material properties

3.6.1 Foam density

The density of foam directly determines the mechanical behaviour of the foam, see Fig. 31 for foam stress-strain relations and the effect of foam density. In our study, different foam densities, i.e., $25\,kg/m^3$, $80\ kg/m^3$ and $180\,kg/m^3$, were used in parametric study. The same triangle pulse was applied to FE helmet-head models with different foam densities. The coup and contrecoup pressure, relative displacement (distance between the surface and the bottom of the frontal foam which is under the impact site in the impact direction), contact pressure (on the surface of head under the impact site), and strain energy of the elements of foam under the impact site were used to study the effect of using different foams. The results are plotted in Figs. 35 – 39.

The major function of the foam during the impact process is to absorb impact energy. Fig. 37 shows that foam with lower density has the larger relative displacement, as a result much more of the strain energy is absorbed by the lower density foam (see Fig. 39), and the amount of mechanical energy transmitted to the head is lower. Intracranial pressures,

i.e., coup pressure and contrecoup pressure, increase with increased foam density (see Fig. 35 and Fig. 36). The helmet-head system with higher density foam has larger maximum von Mises strain during the whole impact process, and thus has higher risk of injury (see Table 7). This can be explained by the relative displacement and contact pressure time history from the impact process. Lower density foam undergoes larger relative displacement (Fig. 37), and more mechanical energy is absorbed by this larger deformation. From Fig. 38, it can be seen that higher density foam would produce a higher contact stress; and a larger reaction force is acted on the head. Contact pressure is directly related to mechanical energy transmitted to the head. Higher contact stress therefore means more mechanical energy will be transmitted to the head. However, it doesn't mean the lower the foam density, the better the helmet will be. A foam that has lower density experiences larger displacement during impact. If the impact force is large enough, the foam would crush completely and the composite shell would touch the head, and it will result in a very large contact force.

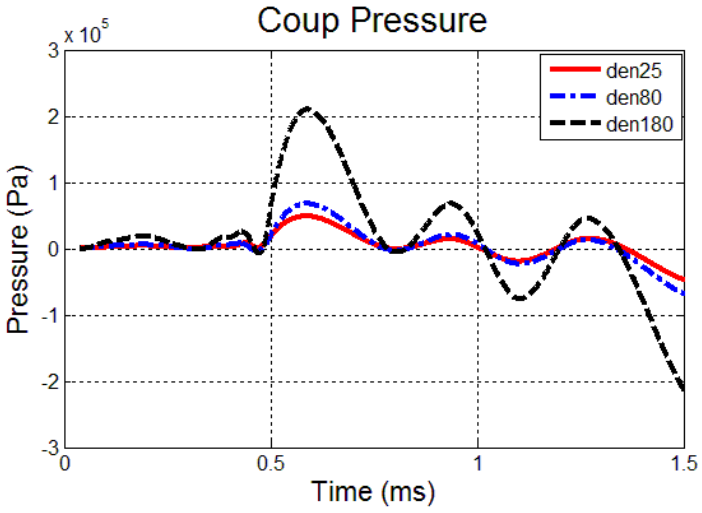

Fig. 35 Coup side pressure histories corresponding to different foam densities

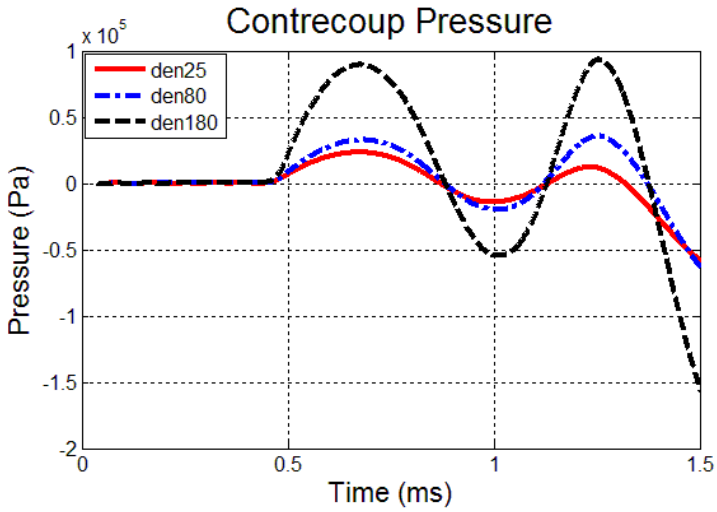

Fig. 36 Contrecoup side pressure histories corresponding to different foam densities

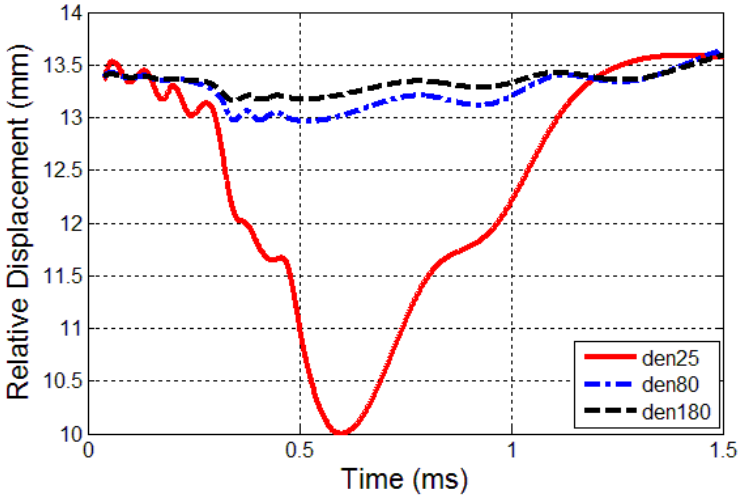

Fig. 37 Relative displacement time histories of different foam densities

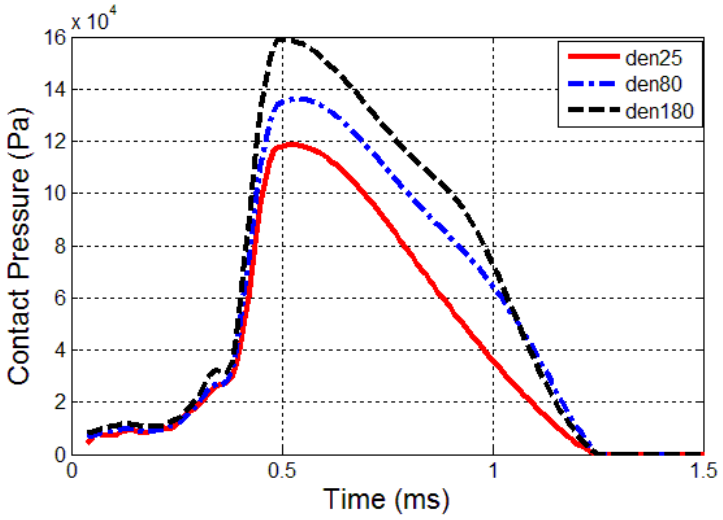

Fig. 38 Contact pressure time histories of different foam densities

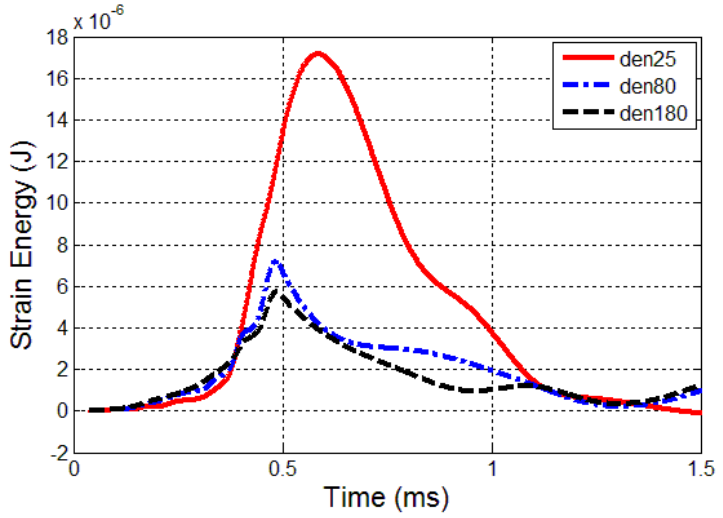

Fig. 39 Strain energy absorbed by foams with different densities

Table 7 Comparison of maximum von Mises strain with different foam densities

	Den25	**Den80**	**Den180**
Maximum von Mises strain	0.02531	0.033	0.0397

3.6.2 Foam thickness

Pad thickness of the helmet is also an important factor that should be considered in helmet design. In this section, different thicknesses of foam, i.e., 10 mm, 15 mm, and 20 mm, were used in parametric studies. The obtained intracranial pressures from three cases are close to each other; however, the case with a thickness 20 mm has the lowest pressure (see Figs. 40 and 41). A change in pad thickness does affect intracranial pressure; a larger thickness would result in a lower intracranial pressure. However, helmet weight would also increase with increasing thickness. A heavier helmet would cause other types of injuries, e.g. neck injury. Significant differences were found in the absorbed strain energy and the contact stress in the three different thicknesses. Fig. 42 shows that the strain energy absorbed by finite elements of foam under the impact site increases with increased foam thickness. This can be explained as the mechanical energy dissipates when the mechanical wave travels through the liner. As a result, larger contact pressure exists in the foam of 10 mm (Fig. 43). Contact duration for the case of 10 mm thickness is about 1.2 ms, while for the other two it is about 0.8 ms. The longer the contact duration, the more impact energy will be transferred to the head. The maximum von Mises strain of the head for the foam thickness 10mm is much larger than in the case of foam thickness 20 mm (Table 8).

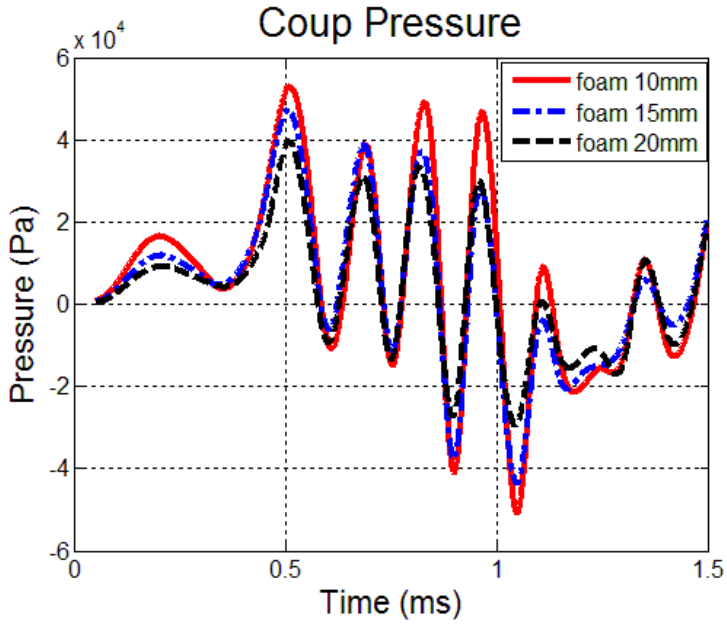

Fig. 40 Coup pressure time histories with different foam thicknesses

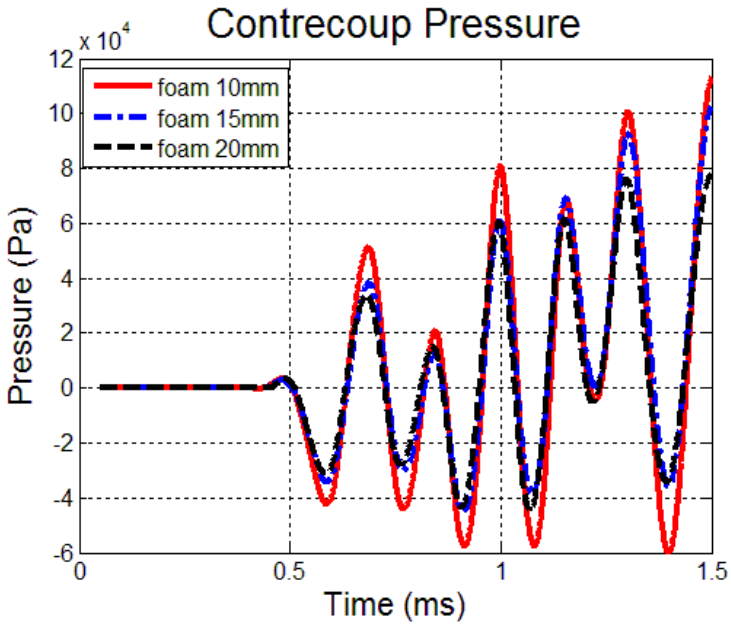

Fig. 41 Contrecoup pressure time histories with different foam thicknesses

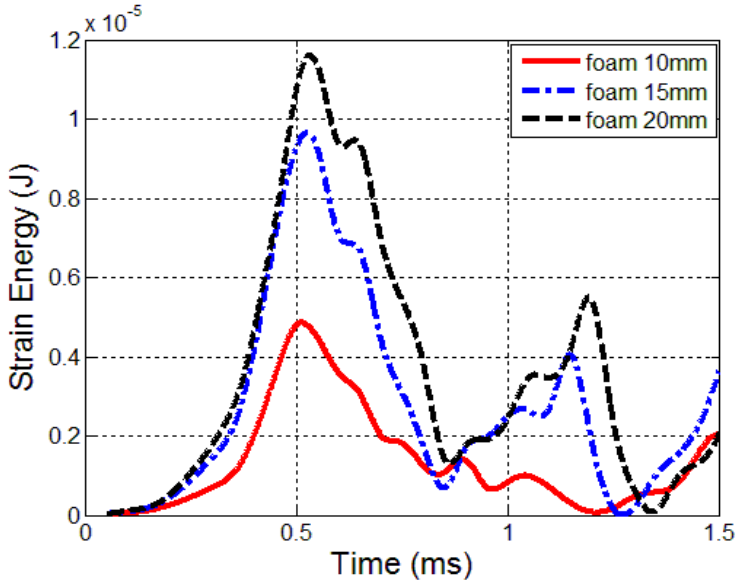

Fig. 42 Strain energy time histories with different foam thicknesses

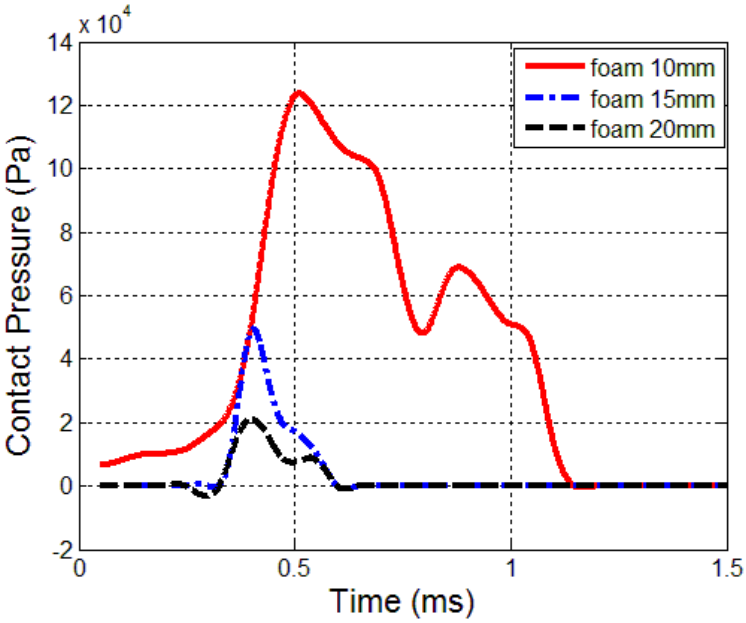

Fig. 43 Contact pressure time histories with different foam thicknesses

Table 8 Comparison of maximum von Mises strain due to different liner thicknesses

	Liner 10mm	**Liner 15mm**	**Liner 20mm**
Maximum von Mises strain	0.033	0.0293	0.0195

3.7 Conclusions

Comparative studies on the effect of different mechanical properties of helmet component on the dynamic head responses were performed. A helmet could effectively decrease the intracranial pressure in the head, thus the possibility of head injuries are decreased. The primary functionality of outmost layer shell is to provide protection against foreign object penetration. Three different composite materials that are commonly in manufacturing helmets were employed to investigate their effects on the overall dynamic performance of helmets. The advantages of composite shells are to absorb energy through failure. However, in the conducted parametric studies, due to the similarity of shear modulus and exclusion of microscopic failure mechanism, the coup and contrecoup intracranial responses of the head were almost the same.

The main energy absorption mechanism of a helmet is to through the permanent deformation of the foam liner. Mechanical properties of the foam are closely related to its thickness and density. The absorbed strain energy by the foam is higher if the foam has a larger thickness and its density is lower. More strain energy would be absorbed if the foam experiences larger displacement during impact. However, if the displacement is too large, it is possible that the inner side of the composite shell will impact the head, and transmits high impact energy to the head. Therefore, in optimal design of helmets, foam thickness and density, as well as the composite shell stiffness should be considered.

Chapter 4

Discussion and Future work

4.1 Summary & Conclusions

In this thesis, we first gave a brief review on different FE models of the human head. The methods used in the literature for constructing FEHMs can be classified into surface-based methods and voxel-based methods. The first step in these methods is geometric segmentation, in which different tissues of the head are separated. The boundary surface of each component in the surface-based method and the localizations of voxels in the voxel-based method have to be determined. Tissue components are refined as detailed as possible to improve the geometric biofideltiy of FEHM. A large amount of manual operations are required in these methods. Both of the methods are suffered from the mesh quality problem as the geometry of the components is very complex. For example, the surface of the cortex is irregular and has very complex geometry. But it is usually simplified as smooth surface to improve the mesh quality in the conventional FEHMs. However, the uneven surface influences the stress/strain distribution inside the brain. The FEHM proposed in this thesis improved mesh quality without losing geometric biofidelity. The detailed anatomic structure of the head was represented by the corresponding material dis-

tributions instead of composing different tissue components separately. This procedure avoided the cumbersome geometric modeling work.

Another improvement in the proposed FEHM is in material biofidelity. Biological materials are inhomogeneous. However, due to ethical regulations and limitations in the experiment techniques, inhomogeneous mechanical properties of head tissues are not available. The homogeneous material properties are instead assigned to head tissues in conventional FEHMs. With the aid of CT images, inhomogeneous material properties have been assigned to bones. The HU values in a CT image are related to the mechanical properties of the bone by mathematical functions established from experiment data. Assumptions were made in this thesis that the material properties of soft tissues are correlated to HU values in a similar way. In the proposed FEHM, head tissues were divided into four main parts, the co-relations between HU values and mechanical properties for each part were established based on experiment data available in the literature. As no such function exists in the literature for the soft tissue, similar correlation functions were assumed for soft tissues. The proposed FEHM was validated by the experimental intracranial pressure reported in the literature. Good agreements were observed. The thin layer of CSF was modelled as solid elements with 'soft' mechanical properties. The ability of the proposed FEHM in simulating large shear strains was examined by applying angular acceleration. Observed from the simulations, there were large stresses/strains existed in the CSF layer. The influence of inhomogeneous material properties on the dynamic responses of the head to impact was also examined by comparing the results with those obtained from homogeneous material model. The model with inhomogeneous material properties re-

vealed much larger maximum peak stress/strain during the impact. The results suggested that using a homogeneous material model would underestimate the injury predictive ability of the FEHM.

Helmet is proved effective in protecting the head from injuries. Parametric studies were conducted to investigate the influences of shell stiffness, foam density and pad thickness on the performance of the helmet in reducing head injuries. Lower foam density and larger liner thickness absorbed more mechanical energy during impact. Contact stress had a higher value if foam density is higher or liner thickness is smaller. The same observations were also found in the coup and contrecoup pressure. The stiff shell serves as a protector of the brain from foreign object penetration. Owing to the advantages of fibre-reinforced composite materials, e.g. high strength-weight ratio, they are widely used in manufacturing helmets. The three commonly used fibre-reinforced materials were considered in parametric studies. Microscopic failure mechanism of composite material was not considered in the simulation. Composite materials reinforced by three types of fibres, i.e., carbon fibre, glass fibre and Kevlar fibre, were considered in the parametric studies. Although these fibres introduced significant differences in the in-plane material properties of the composites, the shear modulus were very similar. Both of the above reasons accounted for the similarity in the intracranial responses of the head.

4.2 Future work

Finite element modeling has become a more and more powerful tool in studying brain injuries. Intracranial stresses/strains are direct causes leading to various brain injuries.

However, in the research reported in this thesis, injury criterion was not covered. In the next step studies, head injury criteria such as Head Injury Criterion, Head Injury Power will be introduced and implemented in the FEHM. After intracranial stresses/strains are obtained by FE simulations, the regions where injury may occur will be identified.

The inhomogeneous material properties of the head tissue were implemented by assigning different mechanical parameters on the FE nodes. Due to the lack of the direct experimental data on the soft tissue brain, the correlations between mechanical parameters of the brain and its HU values were established by making specific assumption. These equations need to be further proved by the experiment. The viscoelasticity behavior of the brain was considered in this research; however, in order to be compared with the experimental data and save the computational efficiency, the impact time (15 ms) is smaller than the decay time (14 s). The viscoelasticity of the brain didn't play significant role on the impact behavior of the brain in our research. For the further research on the mechanisms of brain injury, the simulation time need to large enough to consider the viscoelasticity of the brain.

The protection performance of a helmet is related to its liner and shell. Although a lower foam density and a larger pad thickness absorbed more energy, it doesn't mean there is no limit. A soft liner made of low density foam would experience very large displacement; therefore, it is possible that the inner side of the shell would touch the head. On the other hand, helmet weight would increase if the thickness of the liner is increased. Severe injury would happen to the neck due to the large helmet weight. So an optimization algorithm will be introduced in the future to achieve an optimal design of helmets. All major pa-

rameters will be considered to achieve an overall optimal helmet performance, e.g. lighter weight, higher stiffness and better energy absorption.

The main advantage of fibre reinforced composites is their high stiffness and the mechanism of absorbing mechanical energy by microscopic level damages. In the future version of the helmet model, micro-structural failure models of the fibres and the matrix will be introduced to investigate their effectiveness in further reducing brain injuries.

Bibliography

[1] *Brain injury mechanism*. Available: http://www.braininjury.com/injured.shtml

[2] WISQARS. (2001). *Leading Causes of Death Report, in Web-based Injury Statistics Query and Reporting System (WISQARS), Centers for Disease Control and Prevention*. Available: http://webapp.cdc.gov/sasweb/ncipc/leadcaus.html.

[3] Dougherty, L., Ross, K., Afshar,P., Margulies, S. S., Measurements of intracranial tissue distortion during rapid angular motions. In *CDC-Proceedings: Injury Prevention through biomechics*, Michigan, U. S. A., 1999, pp. 85-94.

[4] Viano, D., Aldman, B., Pape, K., van Hoof, J., and von Holst, H., Brain kinematics in physical model tests with translational and rotational acceleration. *International Journal of Crashworthiness,* vol. 2, pp. 191-206, 1997.

[5] Finkelstein, E., Corso, P. S., Miller,T. R., Ed., *The incidence and economic burden of injuries in the United States*. New York: Oxford University Press, 2006, p.^pp. Pages.

[6] Lin, M.-R. and Kraus, J. F., A review of risk factors and patterns of motorcycle injuries. *Accident Analysis & Prevention,* vol. 41, pp. 710-722, 2009.

[7] *Basic head structure*.

[8] Kleiven, S., Finite element modeling of the human head. Ph. D, Department of Aeronautics, Royal Institute of Technology, Stockholm, 2002.

[9] *Section view of human head*. Available: http://www.fmrib.ox.ac.uk/education/fmri/images/sagittal_scan.jpg/view

[10] Davis, A. E., Mechanisms of traumatic brain injury: biomechanica, structural and cellular considerations. *Critical Care Nursing Quarterly,* vol. 23(3), pp. 1-13, 2000.

[11] Melvin, J. W., Lighthall, J. W., Ueno, K., Ed., *Brain Injury Biomechanics, in Accidental Injury. Nahum, A. M. and Melvin, J. W. (eds),* . New York: Springer-Verlag 1993, p.^pp. Pages.

[12] Hardy, W., Khalil, T., and King, A., Literature review of head injury biomechanics. *International Journal of Impact Engineering,* vol. 15, pp. 561-586, 1994.

[13] Huang, H. M., Finite element analysis of brain contusion: an indirect impact study. *Medical & Biological Engineering & Computing,* vol. 38, 2000.

[14] Brennen, C. E., Cavitation in biological and bioengineering contexts. In *Fifth International Symposium on Cavitation*, Osaka, Japan, 2003, pp. 1-4.
[15] Holbourn, A. H., Phil, D., The mechanics of brain injuries. *British Medical Bulletin*, vol. 3(6), pp. 147-149, 1945.
[16] Luo, Y., Zhang, Q., Del Bigio, M., Recent progress in application of FEM in study of non-penetrating brain injuries. *Advances in Theoretical and Applied Mechanics*, vol. 1(5), pp. 225-240, 2008.
[17] Satoshi, F., Yasuyoshi, Y., Tatsushige, F., Yasuhiko, M., Yoshitsugu, T., Studies on cerebral contusion in the fatal cases by blow, fall and fall down. *The Japanese Journal of Legal Medicine*, vol. 40, pp. 377-383, 1986.
[18] Edberg, S., Rieker, J., Angrist, A., Study of impact pressure and acceleration in plastic skull models. *Lab Investigate*, vol. 12, pp. 1305-1311, 1963.
[19] Stalhammar, D., Olsson, Y., Experimental brain damage from fluid pressures due to impact acceleration. 3. Morphological observations. *Acta Neurol Scand*, vol. 52(1), pp. 38-55, 1975.
[20] *Diffuse Axonal Injury*. Available: http://www.clinical-mri.com/pdf/Essentials%20of%20Clinical%20MR/c16.pdf
[21] King, A. I., Yang, H., Zhang, L. Y., Hardy, Warren, Is head injury caused by linear or angular acceleration? In *International Research Council on the Biomechanics of Injury*, Lisbon (Portugal), 2003.
[22] Baghaei, S. M., Sadegh, A. M., Rajaai, S. M., A Mathematical head/brain model for investigation of damping characteris of SAS in low velocity head impacts. presented at the 25th Southern Biomedical Engineering Conference, Miami, Florida, USA, 2009.
[23] Young, P., An analytical model to predict the response of fluid-filled shells to impact—a model for blunt head impacts. *Journal of Sound and Vibration*, vol. 267, pp. 1107-1126, 2003.
[24] Heydari, M., Jani, Saeid, An ellipsoidal model for studying response of head impacts. *Acta of Bioengineering and Biomechanics*, vol. 12(1), pp. 47-53, 2010.
[25] Wood, J. L., Dynamic response of human cranial bone. *Journal of Biomechanics*, vol. 4, pp. 1-12, 1971.
[26] Ward, C. C. and Thompson, R. B., The Development of a Detailed Finite Element Brain Model. In *Stapp Car Crash Conference*, 1975.
[27] Ward, C. C., Finite Element Models of the Head and Their Use in Brain Injury Research. In *Proceeding of 26th Stapp Car Crash Conference, Society of Automotive Engineers*, Ann Arbor, Michigan, 1982, pp. 71-85.
[28] Ruan, J. S., Khalil, T. B., and King, A. I., Finite Element Modeling of Direct Head Impact. In *Stapp Car Crash Conference*, San Antonio, CA, 1993.
[29] Zhou, C., Khalil, T. B., King, A. I., A new model comparing impact response of the homogeneous and inhomogeneous human brain. In *Proceedings of The 39th Stapp Car Crash Conference*, san Diego, California, USA, 1995.
[30] Nahum, A. M., Smith, R., and Ward, C. C., Intracranial pressure dynamics during head impact. In *Proceedings of the 21st Stapp Car Crash Conference*, 1977.

[31] Zhang, L., Yang, K. H., Dwarampudi, R., Omori, K., Li, T., Chang, K., Hardy, W. N., Khalil, T., and King, A., Recent advances in brain injury research: a new human model development and validation. In *Proceedings 45th Stapp Car Crash Conference*, 2001, pp. 375-400.

[32] Kang, H. S., Willinger, R., Daiw, B. M., and Chinn, B., Validation of a 3D human head model and replication of head impact in motorcycle accident by finite element modeling. In *Proceedings of the 41th Stapp Car Crash conference*, Lake Buena Vista, USA, 1997, pp. 329-338.

[33] Deck, C., Nicolle, S., and Willinger, R., Human head FE modeling: improvement of skull geometry and brain constitutive laws. In *The 4th International Forum of Automotive Traffic Safety*, Changsha, China, 2005.

[34] Kleiven, S. and Hardy, W. N., Correlation of an FE model of the human head with local brain motion-consequences for injury prediction. *Stapp Car Crash Journal,* vol. 46, pp. 123-144, 2002.

[35] Takhounts, E. G., Crandall, J. R., and Darvish, K., On the development of the SIMon Finite Element Head Model. *Stapp Car Crash Journal,* vol. 47, pp. 107-133, 2003.

[36] Zong, Z., Lee, H. P., and Lu, C., A three-dimensional human head finite element model and power flow in a human head subject to impact loading. *Journal of Biomechanics,* vol. 39, pp. 284-292, 2006.

[37] Watanabe, D., Yuge, K., Nishimoto, T., Murakami, S., and Takao, H., Head Impact Analysis related to the Mechanism of Diffuse Axonal Injury. 2008.

[38] Chen, Y. and Ostoja-Starzewski, M., MRI-based finite element modeling of head trauma: spherically focusing shear waves. *Acta Mechanica,* vol. 213, pp. 155-167, 2010.

[39] Bandak, F. A., Vander Vorst, M. J., Stuhmiller, L. M., Mlakar, P. F., Chilton, W. E., and stuhmiller, J. H., An imaging-based computational and experimental study of skull fracture: finite element model development. *Journal of Neurotrauma,* vol. 12(4), pp. 679-688, 1995.

[40] Chu, C. S., Lin, M. S., Huang, H. M., and Lee, M. C., Finite element analysis of cerebral contusion. *Journal of Biomechanics,* vol. 27(2), pp. 187-194, 1994.

[41] Ruan, J. S., Khalil, T., and King, A., Impact head injury analysis using an explicit finite element human head model. *Journal of traffic medicine,* vol. 25, 1997.

[42] Dimasi, F., Marcus, J., and Eppinger, R., 3-D anatomic brain model for relating cortical strains to automobile crash loading. In *Proceedings of the 13th International Technical conference on Experimental Safety Vehicles*, 1991.

[43] Kuijpers, A. H., claessens, M. H., and Sauren, A. A., The influence of different boundary and interface conditions on the response of the head to impact: a two-dimensional finite element study. *Journal of Neurotrauma,* vol. 12(4), pp. 715-724, 1995.

[44] Ueno, K., Melvin, J. W., Li, L., and Lighthall, J. W., Development of tissue level brain injury criteria by finite element analysis. *Journal of Neurotrauma,* vol. 12(4), pp. 695-706, 1995.

[45] Claessens, M. H., sauren, F., and Wismans, J., Modeling of the human head under impact conditions: a parametric study. In *Proceedings of the 41st Stapp Car Crash Conference,*, 1997, pp. 315-328.
[46] DiMasi, F. P., Eppinger, R. H., and Bandak, F. A., Computational Analysis of Head Impact Response Under Car Crash Loadings. *SAE Paper952718*, 1995.
[47] Khalil, T., Comparison of human skull and spherical shell vibrations—implications for head injury modeling. *Journal of Sound and Vibration*, vol. 82, pp. 95-110, 1982.
[48] Willinger, R., Kopp, C. M., and Cesari, D., Cerebral motion and head tolerance. In *35the Proceedings of the Association for the Advancement of Automotive Medicine (ISSN)*, Toronto, 1991, pp. 387-404.
[49] Trosseille, X., Tarriére, C., Lavaste, F., Guillon, F., and Domont, A., Development of a F.E.M. of the Human Head According to a Specific Test Protoco. In *30th Stapp Car Crash Conference*, Seattle, WA, USA, 1992, pp. 235-253.
[50] Willinger, R., Kang, H. S., and Daiw, B. M., Three-dimensional human head finite-element model validation against two experimental impacts. *Annals of Biomedical Engineering*, vol. 27(3), pp. 403-410, 1999.
[51] Hardy, W. N., Foster, C. D., Mason, M. J., Yang, K. H., and Tashman, S., Investigation of head injury mechanisms using neutral density technology and high-speed biplanar x-ray. *Stapp Car Crash Journal*, vol. 45, pp. 337-368, 2008.
[52] Versace, J., A review of the severity index. In *Proceeding of the 15th Stapp Car Crash Conference*, 1971, pp. 771-796.
[53] Hertz, E., A note on the head injury criterion (HIC) as a predictor of the risk of skull fracture. presented at the 37th Annual Proceedings of the AAAM, 1993.
[54] Newman, J. A., Head Injury Criteria in Automotive Crash Testing. In *Proceedings of the 27th Stapp Car Crash Conference*, 1980, pp. 701-747.
[55] Newman, J. A., Shewchenko, N., and Welbourne, E., A proposal new biomechanical head injury assessment function -the maximum power index. *Stapp Car Crash Journal*, vol. 44 pp. 215-247, 2000.
[56] Ho, J., von Holst, H., and Kleiven, S., Automatic generation and validation of patient-specific finite element head models suitable for crashworthiness analysis. *International Journal of Crashworthiness*, vol. 14, pp. 555-563, 2009.
[57] Khurshid, A., Ghafoor, A., and Malik, M. A., Effects of Material Properties on Soft Contact Dynamics. *Key Engineering Materials*, vol. 442, pp. 438-444, 2010.
[58] Findley, W. N., *Creep and relaxation of nonlinear viscoelastic materials, with an introduction to linear viscoelasticity*: North-Holland Pub. Co. : sole distributors for the U.S.A. and Canada, Elsevier/North Holland, 1976.
[59] Flugge, W., *Viscoelasticity* 2ed.: Springer-Verlag, 1975.
[60] Davis, G., Kohandel, M., Sivaloganathan, S., and Tenti, G., The constitutive properties of the brain paraenchymaPart 2. Fractional derivative approach. *Medical Engineering & Physics*, vol. 28, pp. 455-459, 2006.
[61] Zener, C., *Elasticity and Anelasticity of Metals*: Chicago University Press, 1948.

[62] Schiessel, H., Metzler, R., Blumen, A., and Nonnenmacher, T. F., Generalized viscoelastic models: their fractional equations with solutions. *Journal of Physics A: Mathematical and Theoretical,* vol. 28, pp. 6567-6584, 1995.
[63] Atanackovic, T. M., A modified Zener model of a viscoelastic body. *Continuum Mechanics and Thermodynamics,* vol. 14, pp. 137-148, 2002.
[64] Pritz, T., Analysis of Four-Parameter Fractional Derivative Model of Real Solid Materials. *Journal of Sound and Vibration,* vol. 195, pp. 103-115, 1996.
[65] ANSYS Structural analysis menu.
[66] Helgason, B., Taddei, F., Palsson, H., Schileo, E., Cristofolini, L., Viceconti, M., and Brynjolfsson, S., A modified method for assigning material properties to FE models of bones. *Medical Engineering & Physics,* vol. 30, pp. 444-453, 2008.
[67] Gupta, S. and Dan, P., Bone Geometry and Mechanical Properties of The Human Scapula Using Computed Tomography Data. *Trends in Biomaterials & Artificial Organs,* vol. 17(2), pp. 61-70, 2004.
[68] Kopperdahl, D. L., Morgan, E. F., and Keaveny, T. M., Quantitative computed tomography estimates of the mechanical properties of human vertebral trabecular bone. *Journal of Orthopaedic Research,* vol. 20, pp. 801-805, 2002.
[69] Keyak, J. H., Lee, I. Y., and Skinner, H. B., Correlations between orthogonal mechanical properties and density of trabecular bone: use of different densitometric measures. *Journal of Biomedical Materials Research,* vol. 28(11), pp. 1329-1336, 1994.
[70] Majumder, S., Roychowdhury, A., and Pal, S., Simulation of hip fracture in sideways fall using a 3D finite element model of pelvis–femur–soft tissue complex with simplified representation of whole body. *Medical Engineering & Physics,* vol. 29, pp. 1167-1178, 2007.
[71] Snyder, S. M. and Schneider, D. E., Estimation of mechanical properties of cortical bone by computed tomography *Journal of Orthopaedic Research* vol. 9(3), pp. 422-431, 1991.
[72] Dalstra, M., Huiskes, R., Odgaard, A., and van Erning, L., Mechanical and textural properties of pelvic trabecular bone. *Journal of Biomechanics,* vol. 26 (4/5), pp. 523-535, 1994.
[73] Taddei, F., An improved method for the automatic mapping of computed tomography numbers onto finite element models. *Medical Engineering & Physics,* vol. 26, pp. 61-69, 2004.
[74] Perillo-Marcone, A., Alonso-Vazquez, A., and Taylor, M., Assessment of the Effect of Mesh Density on the Material Property Discretisation Within QCT Based FE Models: A Practical Example Using the Implanted Proximal Tibia. *Computer Methods in Biomechanics and Biomedical Engineering,* vol. 6, pp. 17-26, 2003.
[75] Zannoni, C. and Mantovani, R. V., M., Material properties assignment to finite element models of bone structures: a new method. *Medical Engineering & Physics,* vol. 20, pp. 735-740, 1998.
[76] Schileo, E., Dall'Ara, E., Taddei, F., Malandrino, A., Schotkamp, T., Baleani, M., and Viceconti, M., An accurate estimation of bone density improves the accuracy

of subject-specific finite element models. *Journal of Biomechanics,* vol. 41, pp. 2483-2491, 2008.

[77] Chen, G., Schmutz, B., Epari, D., Rathnayaka, K., Ibrahim, S., Schuetz, M. A., and Pearcy, M. J., A new approach for assigning bone material properties from CT images into finite element models. *Journal of Biomechanics,* vol. 43, pp. 1011-1015, 2010.

[78] Kluess, D., Souffrant, R., W., M., Wree, A., Schmitz, K. P., and Bader, R., A convenient approach for finite-element-analyses of orthopaedic implants in bone contact: modeling and experimental validation. *Computer Methods and Programs in Biomedicine,* vol. 95(1), pp. 23-30, 2009.

[79] Kleiven, S. and Von Holst, H., Consequences of head size following trauma to the human head. *Journal of Biomechanics,* vol. 35(2), pp. 153-160, 2002.

[80] McLean, A. J. and Anderson, W. G. R., Biomechanics of closed head injury. *Biomechanics Its Foundations and Objectives,* pp. 25-38, 1997.

[81] Pinnoji, P. K. and Mahajan, P., Finite element modelling of helmeted head impact under frontal loading. *Sadhana,* vol. 32(4), pp. 445-458, 2007.

[82] van Hoof, J., Cronin, D. S., Worswick, M. J., Williams, K. V., and Nandlall, D., Numerical head and composite helmet models to predict blunt trauma. In *19th International Symposium of Ballistics,* Interlaken, Switzerland, 2001, pp. 921-928.

[83] Kostopoulos, V., Markopoulos, Y. P., Giannopoulos, G., and Vlachos, D. E., Finite element analysis of impact damage response of composite motorcycle safty helmets. *Composites: Part B,* vol. 33, pp. 99-107, 2002.

[84] viot, P., Maheo, L., and Mercier, A., Behaviour of polymeric multiscale foam under dynamic loading-study of the influence of the density and the walls of beads. *International Journal of Research and Reviews in Applied Sciences,* vol. vol. 7(1), pp. 1-19, 2011.

[85] Viot, P., Hydrostatic compression on polypropylene foam. *International Journal of Impact Engineering,* vol. 36, pp. 975-989, 2009.

[86] Laura B. Drew, W. E. D., The Contrecoup-coup Phenomenon A new understanding of the mechanism of closed head injury. *Neurocritical Care,* vol. 1(3), pp. 385 - 390, 2004.